Angular momentum transfer in the reactions induced by 166 MeV ^{20}Ne on ^{63}Cu

R. A. Dayras,* R. G. Stokstad,† D. C. Hensley, and M. L. Halbert
Oak Ridge National Laboratory, Oak Ridge, Tennessee 37830

D. G. Sarantites and L. Westerberg‡
Department of Chemistry, Washington University, St. Louis, Missouri 63130

J. H. Barker
Department of Physics, St. Louis University, St. Louis, Missouri 63103

(Received 17 March 1980)

A study has been made of the energy, angular, and charge distribution of products emitted in the reaction of 166-MeV ^{20}Ne ions with ^{63}Cu. The first three moments of the γ-ray multiplicity distribution and the out-of-plane γ-ray angular correlations have been measured in coincidence with the projectile-like fragments. Relaxation times of 2.6×10^{-22} s for energy dissipation, 4.1×10^{-22} s for angular momentum transfer, and a charge diffusion coefficient of 0.58×10^{22} (charge units)^2 s^{-1} have been deduced from these data. A small γ-ray anisotropy and a large width of the multiplicity distribution have been observed. These are interpreted in terms of a random component of transferred angular momentum whose magnitude is comparable to that of the aligned component induced by tangential friction. Thermal excitation of collective modes of motion in the equilibrated dinuclear complex can account quantitatively for these experimental results. Other mechanisms for the generation of a random component of angular momentum are also possible.

[NUCLEAR REACTIONS ^{63}Cu(^{20}Ne,X), X=deeply inelastic fragments, evaporation residues, E=166 MeV, enriched target; measured $\sigma(E,\theta,Z)$, γ-ray multiplicity, angular correlations; deduced relaxation times, diffusion coefficients, random angular momentum. ^{63}Cu(^{12}C,X), X=evaporation residues, E=133 MeV, measured γ-ray multiplicity.]

I. INTRODUCTION

The study of strongly damped collisions for a variety of systems has led to the concept of a short-lived, rotating dinuclear complex which, after a large damping of the initial kinetic energy of relative motion, separates into projectile-like and target-like fragments.[1,2] Recent experiments show that the fragments share, according to their relative masses, an excitation energy determined by the degree of damping of the initial relative motion.[3-7]

Until recently, experimental information was obtained mainly from measurements of the kinetic energy, mass, charge, and differential cross section of the final reaction products. From these measurements, it has been established that energy damping and mass exchange increase with the amount of rotation (or lifetime) of the dinuclear complex. These aspects of strongly damped collisions are relatively well explained by classical equations of motion including dissipative terms and a diffusion process based on the Fokker-Planck equation.[8-11]

However, the preceding types of experiments and classical analyses address only indirectly the nature of the frictional forces which convert kinetic energy of relative motion into internal excitation energy. Measurements of the energy loss alone are sensitive mainly to the radial component of the friction force. On the other hand, measurements of the angular momentum imparted to the final fragments probe more directly the role played by tangential friction during the collision. Such measurements can determine whether this frictional force is sufficient to lead to the formation of rigid body within the collision time or whether the surfaces of the colliding nuclei retain some relative motion at the time of scission. This, in turn, may furnish some clue to the one- or two-body nature of these forces. Furthermore, a knowledge not only of the magnitude, but also of the distribution and alignment of the transferred angular momentum can provide a more stringent test of different models proposed for angular momentum dissipation in deeply inelastic scattering.

It has been found experimentally that the amount of angular momentum transferred to the fragments in completely relaxed collisions is approximately consistent with the formation of a rigid intermediate dinuclear complex (termed "the sticking limit").[12-19] However, the surprisingly large values measured for the width σ_γ of the γ-ray multiplicity distribution,[20-22] the values of the out-of-plane total γ-ray anisotropy A (Refs. 14, 18, 22–26) as well as results of the γ-ray polarization

measurements,[25,27] suggest that the alignment of the angular momenta of the fragments may be less than that given by the classical picture of rigid rotation. There are, however, several other effects which might be responsible for the experimental observations. The most obvious is the emission of light particles (p,n,α) by the excited fragments. Although this effect can be an important contribution to the misalignment deduced from an analysis of the subsequent γ-ray emission, we will see that it is not sufficient to explain the present experimental data. It has been shown recently that statistical fluctuations in the magnitude of the angular momentum transferred during deep inelastic collisions can be significant.[28] However, calculations including this effect still underestimate the measured γ-ray multiplicity widths by more than a factor od 2.[21,29] Clearly, some other mechanisms must be invoked to interpret the experimental data. It has been suggested,[23,30] by analogy to fission, that collective modes such as twisting, bending, and/or wriggling could be excited in deep inelastic collisions, thereby inducing extra components of angular momentum with a nearly random orientation. In general, there are several possible mechanisms in addition to those just mentioned which could introduce a nonaligned or randomly oriented transferred angular momentum.[31,32]

In order to gain additional information on the mechanisms for angular momentum transfer and, hopefully, to understand the origin of the above discrepancies between experiment and theory, we have undertaken an extensive study of one reaction, 166 MeV ^{20}Ne + ^{63}Cu. Measurements have been made of the energy, charge, and angular distribution of the projectile-like fragments produced in this reaction. In addition, the angular correlations and the first three moments of the multiplicity distribution of γ rays emitted in coincidence with the above products and with evaporation residues were determined. (A study of the emission of protons and α particles in coincidence with the deep inelastic products was also undertaken and will be reported separately.) The experimental results are presented in Sec. III and discussed in Sec. IV. A summary is given in Sec. V. The main conclusion of our study is that a relatively large component of a randomly oriented angular momentum is imparted to the primary fragments. A brief account of this work has appeared previously.[22]

II. EXPERIMENTAL PROCEDURE

A beam of 167.8-MeV ^{20}Ne ions provided by the Oak Ridge Isochronous Cyclotron was used to bombard 1-mg/cm^2-thick targets of ^{63}Cu enriched to 99%. The effective energy of the beam at the center of the target was 166 MeV.

Great care was exercised to determine and verify the possible presence of light contaminants such as carbon and oxygen on the target. To minimize hydrocarbons, the reaction chamber was thoroughly cleaned with acetone and the vacuum was maintained below 10^{-6} Torr with a cryogenic pump. The scattering chamber was isolated from the beam line by a trap cooled with liquid nitrogen. All seals used low vapor pressure O rings. Before being inserted into the chamber each target, consisting of a strip of ^{63}Cu, 5 cm long and 1.5 cm wide, was reduced by prolonged heating in a hydrogen atmosphere. Furthermore, during a run the target was periodically displaced in 6 mm steps such that a given spot on the target was bombarded for only a short time. As a check for the presence of light contaminants, each run was repeated with a carbon target.

An array of 9 NaI(Tl) detectors (5.1 cm×7.6 cm) was operated in coincidence with two heavy-ion telescopes, each consisting of a ΔE gas ionization chamber and a 1500-μm surface barrier E detector. Table I gives the geometrical arrangement of the detectors. The counter telescopes were coplanar with, and located on opposite sides of, the beam. One was used to cover the angular range between 10° and 30° and subtended a solid angle of 3 msr. The other one was used to cover the angular range between 30° and 60° and subtended a solid angle of 9 msr. The counting rates in both detectors were kept approximately equal by an appropriate choice of their relative position.

The NaI detectors were individually shielded and

TABLE I. Experimental arrangement of the detectors. The angles θ and ϕ are defined in a spherical polar coordinate system with its polar axis ($\theta=0$) along the beam direction and its origin at the center of the target. The azimuthal angle ϕ is taken to be zero in the half plane defined by the beam and the heavy ion telescope number 1 (HI-1). The angle α is the polar angle relative to the perpendicular to the reaction plane.

Detector	θ (deg)	ϕ (deg)	α (deg)
HI-1	10–30	0	90
HI-2	30–60	180	90
NaI-1	125	0	90
NaI-2	145	180	90
Nai-3	45	90	45
NaI-4	69.3	49.1	45
NaI-5	110.7	49.1	45
NaI-6	135	90	45
NaI-7	110.7	130.9	45
NaI-8	69.3	130.9	45
NaI-9	90	90	0

their front faces were located 10 cm from the target. In order to attenuate the x rays from the target and the lead shield surrounding the detectors, their thresholds were set at 85 keV, and 0.5 mm Cd and 0.13 mm Cu absorbers were placed in front of each detector. These absorbers also made the total detection efficiency less dependent upon the γ-ray energy. The detectors were calibrated *in situ* with standard sources of ^{107}Cd, ^{57}Co, ^{133}Ba, ^{137}Cs, and ^{60}Co. The average detection efficiency per detector was found to be 0.00465, 0.00945, 0.0112, 0.00933, and 0.00849 at 88, 124, 176, 662, and 1253 keV, respectively. Above 500 keV, the detection efficiency remained practically constant. Crystal-to-crystal scattering was checked with ^{137}Cs and ^{54}Mn sources and found to be negligible. In a separate measurement[33] using a similar geometrical configuration, the detection efficiency of the NaI detectors for neutrons was found to be ~14% of the detection efficiency for 700 keV γ rays. As the average number of neutrons emitted in the present reaction was not known, a separate measurement of the relative yields for neutrons and γ rays in the NaI detectors was made using the time-of-flight method with one of the NaI detectors placed one meter from the target at $\theta = 45°$ in the reaction plane. Since 45° was the most forward angle at which any of the NaI detectors was located, this measurement enabled the determination of an upper limit on the effects of neutron detection for a measurement of the γ-ray multiplicity.

Coincidences between the heavy-ion telescopes and the individual NaI detectors were established by the overlap coincidence technique. Because of the different arrival times in the telescopes of ions with different mass and energy, a rather long resolving time, $2\tau = 100$ ns, was used.

Depending on whether 0, 1, 2, 3, or 4 or more NaI detectors recorded γ rays in coincidence with one or the other of the heavy-ion telescopes, the digitized ΔE and $E + \Delta E$ signals were stored on line in one of two sets of five 300×300 channel arrays. Simultaneously, the linear signals from 4 of the 9 NaI detectors were recorded event-by-event on magnetic tape. Two of these detectors (NaI-1 and NaI-2 of Table I) were located in the reaction plane. The other two detectors (NaI-5 and NaI-9 of Table I) defined a vertical plane oriented at 120° from the beam direction. Measurements were done with the telescopes located at 20°, 26°, 35°, and 45° and projectile-like products with $3 \leq Z \leq 16$ were identified at each angle. Special measurements were made of the γ-ray multiplicity distributions for the evaporation residues. Since the evaporation residues emerge with relatively low energy, the gas pressure in the ionization chambers was decreased by a factor of 2. Measurements were done at 10°, 15°, 20°, and 28°. The yield of events from a pulser (triggered by the beam integrator) in the different $\Delta E - E$ spectra was used to correct for random events. The corrections for randoms were generally small ($\leq$2%) and never exceeded 10%.

III. EXPERIMENTAL RESULTS

A. Charged particle results

1. Cross sections and limiting angular momenta

From a study of the reaction ^{20}Ne +Ni at 169 MeV, Obenshain *et al.*[34] have determined a total reaction cross section $\sigma_R = (2010 \pm 80)$ mb. Neglecting the slight differences in target and bombarding energy, we have adopted the same reaction cross section for the ^{20}Ne + ^{63}Cu reaction. From this value we deduce a grazing angle $\theta_{lab} = 18°$ ($\theta_{c.m.} = 23.7°$) and a grazing angular momentum $l_{gr} = (76 \pm 1)\,\hbar$.

In a separate measurement, we have obtained for the evaporation residues a cross section $\sigma_{ER} = (1276 \pm 80)$ mb, in good agreement with the value (1236 ± 50) mb obtained by Obenshain *et al.*[34] for the reaction ^{20}Ne +Ni. It should be noted that this cross section does not necessarily represent the total fusion cross section as it excludes a possible contribution from fission. In the present experiment, such fission products cannot be distinguished from deep inelastic products producing a nearly symmetric mass split. However, from the liquid-drop fission competition model,[35] one expects such a contribution from equilibrium fission to be small. A critical-distance calculation[36] predicts a fusion cross section $\sigma_{fus} = 1270$ mb, in excellent agreement with our measurement of σ_{ER}. Consequently, we have neglected the possibility of fission and have equated the fusion cross section with the evaporation residue cross section. Using the sharp cutoff approximation, we deduce a critical angular momentum for fusion $l_{cr} = (60 \pm 1)\,\hbar$.

The difference $(734 \pm 120$ mb) between σ_R and σ_{ER} is attributed to deeply inelastic and quasielastic reactions which should be approximately localized in a band of incident partial waves between l_{cr} and l_{gr}.

2. Energy, charge, and angular distributions of the projectile-like fragments

Singles energy spectra were obtained for the projectile-like products with $3 \leq Z \leq 16$ by adding coincidence spectra of all folds. Each spectrum was corrected for pulse height defects using the method proposed by Kaufman *et al.*[37] and was also corrected for energy loss in the target and in the windows of the heavy-ion telescope. The stopping

powers of Northcliffe and Schilling[38] were used.

As we have limited ourselves to measurements near and beyond the grazing angle, it was possible to decompose the energy spectra in an unambiguous way into a quasielastic component and a deeply inelastic component. This is illustrated in Fig. 1 which shows a spectrum of Ne ions at $\theta_{lab} = 26°$. The most probable laboratory energy $\langle E \rangle$ and the full width at half maximum of the deep inelastic component are indicated. The energy width W shows a strong dependence upon the scattering angle and on the Z of the fragment, as indicated in Fig. 2(a). However, the ratio $W/\langle E \rangle$ is remarkably independent of angle [Fig. 2(b)] and decreases with Z from ~0.68 for $Z=3$ to ~0.45 for $Z=10$, where it reaches a constant value. The constancy for a given reaction product of this ratio is indicative of a strong correlation between energy loss and energy spread.

Figure 3(a) shows the mean reaction Q value vs the atomic number of the light product for different scattering angles. As expected, the deep inelastic component shows an energy damping which increases with scattering angle and mass transfer between projectile and target. The Q values shown in Fig. 3(a) were obtained on the assumption that the final state has only two bodies and that the mass A_1 of the detected product with a given Z corresponds to the isotope closest to the line of β stability. This simple approach overestimates the amount of kinetic energy lost in the collision through its neglect of particle emission of the excited fragments. We have made a correction for this effect by using an iterative procedure with the following hypotheses. (i) The primary fragments in the two-body reaction share an amount of excitation energy proportional to their masses and

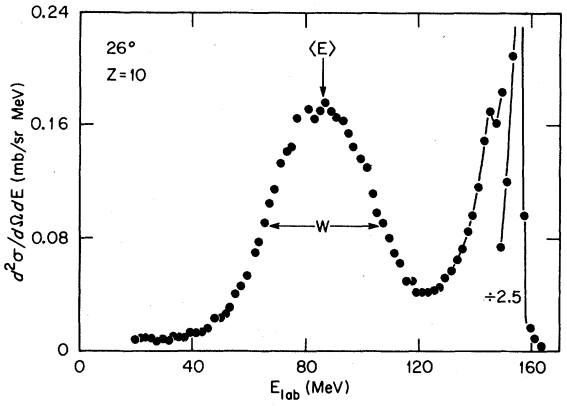

FIG. 1. Energy spectrum of Ne ions produced in the reaction of 166 MeV ^{20}Ne with ^{63}Cu. The scattering angle is 26°. A quasielastic component ($E_{lab} > 120$ MeV) and a deep inelastic component are evident. The quantities $\langle E \rangle$ and W are the most probable energy and the full width at half maximum for the deep inelastic component.

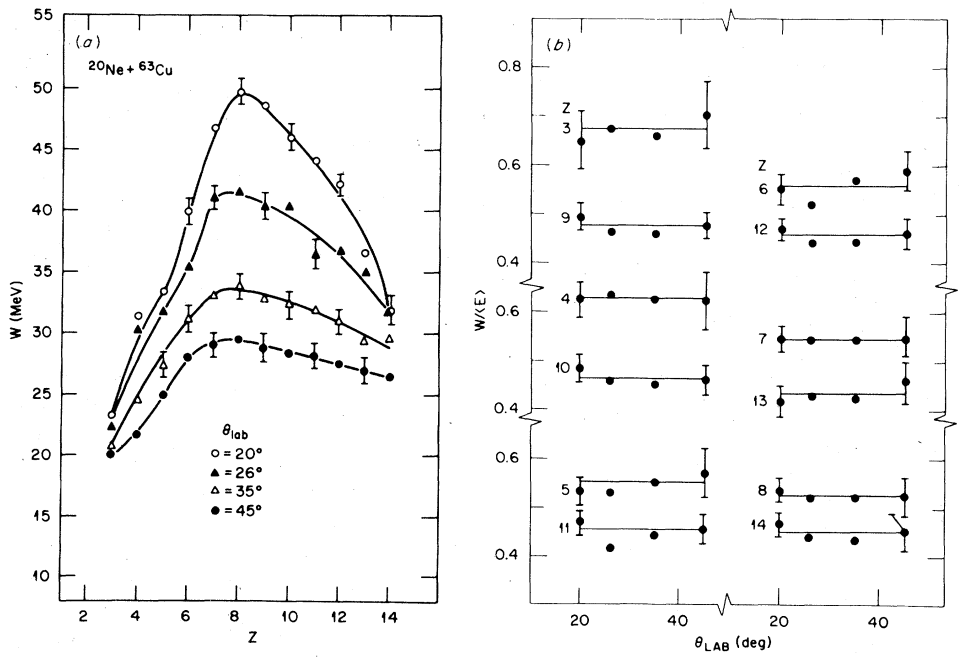

FIG. 2. (a) Energy width of the deep inelastic component as a function of the projectile-like fragment Z, for different scattering angles. (b) Ratio between the energy width and the most probable lab energy of the projectile-like fragment as a function of the scattering angle. The quantities W and $\langle E \rangle$ are defined in Fig. 1. The lines through the data points are to guide the eye.

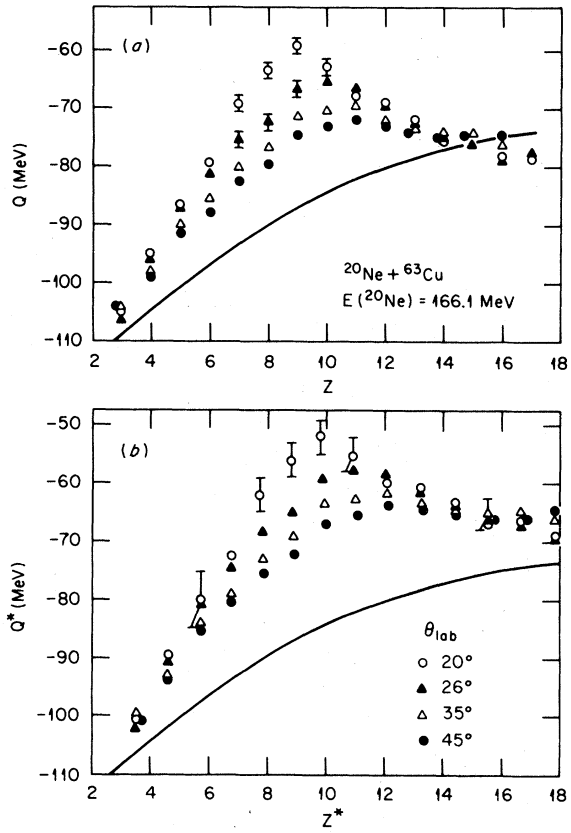

FIG. 3. (a) Reaction Q values determined directly from the measured kinetic energy of the detected fragment with the assumption of two-body kinematics vs the measured Z. (b) Reaction Q values obtained after correcting for particle evaporation (see text) vs the average atomic number Z^* of the primary projectile-like fragments. The curves in (a) and (b) correspond to the Q values expected for two spherical fragments emerging from the collision with a Coulomb repulsion energy given by a radius parameter $r_0 = 1.5$ fm.

an amount of angular momentum proportional to their moments of inertia. (ii) The neutron-to-proton ratio of the primary fragments is equal to the ratio $R = N/Z$ of the composite system. (iii) The light particles are emitted from equilibrated fragments. These hypotheses are generally consistent with available experimental data, although there is evidence for some preequilibrium emission of light particles.[39-42]

The calculation of the mass ΔA_1 evaporated by the projectile-like fragment begins with a first estimate of its average excitation energy $\langle E_{ex}^{(1)} \rangle$ and angular momentum $\langle J_1 \rangle$. The excitation energy $\langle E_{ex}^{(1)} \rangle$ was deduced from the Q values of Fig. 3(a) through the equation

$$E_{ex}^{(1)} = \frac{A_1}{A} \langle Q \rangle , \tag{1}$$

where A_1 is the mass of the detected fragment and A is the total mass of the composite system. A first estimate of the angular momentum $\langle J_1 \rangle$ was deduced from the total angular momentum $\langle J \rangle$ transferred during the collision through the equation

$$\langle J_1 \rangle = \frac{\mathcal{I}_1}{\mathcal{I}_1 + \mathcal{I}_2} \langle J \rangle , \tag{2}$$

where $\langle J \rangle$ was obtained from our γ-ray multiplicity measurements. Assuming spherical shapes for the fragments, the moments of inertia are given by $\mathcal{I}_i = \frac{2}{5} r_0^2 A_i^{5/3}$ ($i = 1$ or 2) with $r_0 = 1.4$ fm. This information was then used in the Monte Carlo statistical-model code JULIAN[43] to determine the average evaporated mass ΔA_1. Neglecting recoil effects, the energy of the primary projectile-like fragment, $\langle E_{1L}^* \rangle$, was expressed as

$$\langle E_{1L}^* \rangle = \frac{A_1 + \Delta A_1}{A_1} \langle E_{1L} \rangle , \tag{3}$$

where $\langle E_{1L} \rangle$ is the average energy of the detected fragment. The energy E_{1L}^* and the mass $A_1 + \Delta A_1$ were then used in a two-body kinematic calculation to determine a new reaction Q value. At this point, the iterative process was repeated, starting from Eq. (1) with the new mass and Q value. Three iterations were generally sufficient to reach convergence. It was found that the average number of nucleons evaporated by the projectile-like fragments increases from ~1.5 for carbon to ~3.5 for sulfur and depends slightly upon the scattering angle. For fragments lighter than carbon, the particle evaporation correction becomes quite uncertain and its effect is probably underestimated.

From the calculated average evaporated mass ΔA_1 and the mass A_1 of the detected fragment, we define an effective atomic number Z^* for the primary fragment through the equation

$$Z^* = \frac{A_1 + \Delta A_1}{R + 1} . \tag{4}$$

The primary Q value $\langle Q^* \rangle$ obtained after correction for light-particle emission, is shown in Fig. 3(b) as a function of the effective atomic number Z^* of the primary fragments. The consequences of particle emission can be readily seen form a comparison of Figs. 3(a) and 3(b).

The center-of-mass differential cross sections $(d\sigma/d\theta)_{c.m.}$, integrated over particle energy for laboratory products with $3 \leq Z \leq 16$, are shown in Fig. 4 for the deeply inelastic component. The effects of light-particle emission have been taken into account in transforming to the center-of-mass system. The forward peaking of the angular distributions for products with Z near that of the pro-

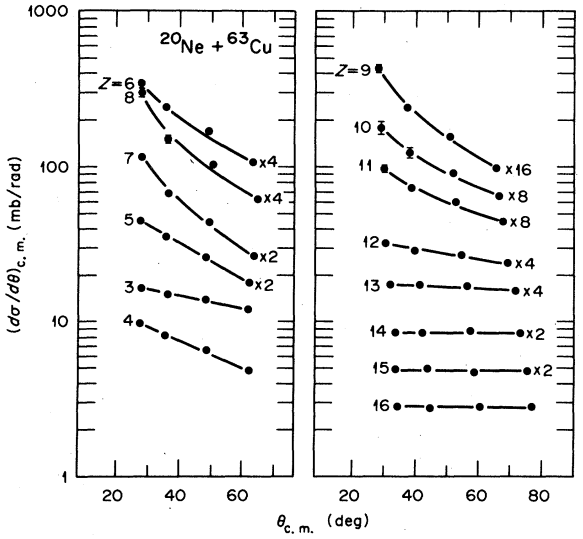

FIG. 4. Center-of-mass differential cross sections $d\sigma/d\theta$, integrated over the energy of the deeply inelastic component, for different Z values of the detected fragments. Statistical errors and errors due to the unfolding procedure are indicated where they are larger than the data points. Absolute errors are estimated to be of the order of ±10%. The lines through the data points are to guide the eye.

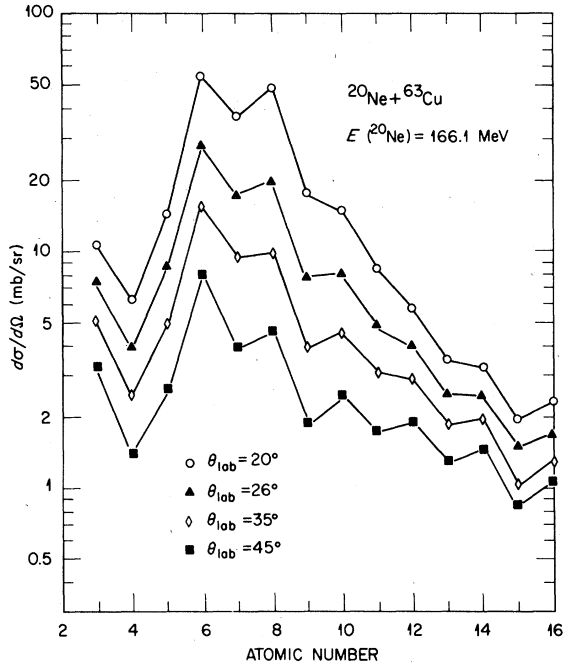

FIG. 5. Z distributions of the observed projectile-like fragments from deeply inelastic collisions. Note the odd-even effect which increases with scattering angle.

jectile is typical of systems for which the modified Sommerfeld parameter[44] $\eta' = Z_p Z_t e^2/\hbar v'$ is small; in our case, $\eta' \sim 20$. Z_p and Z_t are the atomic numbers of the projectile and the target, respectively, and v' is the relative velocity at the interaction barrier. The differential cross sections for products with $Z \geq 13$ are essentially flat and thus they are indistinguishable from cross sections for fission of an equilibrated compound nucleus.

The charge distributions of the detected projectile-like fragments, integrated over energy, are displayed in Fig. 5 for different laboratory scattering angles. These distributions clearly show odd-even effects which become more pronounced at more backward scattering angles. Such an effect has been noticed previously.[34,45,46] We attribute this to light-particle emission from the excited fragments rather than to the primary reaction mechanism, since the particle-emission correction shows a preferential decay of the primary fragments toward even-Z nuclei.

3. *Diffusion-model analysis*

Following Nörenberg,[8] we first decompose the total differential cross section, summed over all Z, into positive and negative scattering angles. This is shown in Fig. 6(a). It has been assumed that the deeply inelastic component is associated with negative scattering angles, whereas the quasielastic component corresponds to positive scattering angles. In Fig. 6(b), the average, $\langle Z \rangle$ and the variance $\sigma_Z^2 = \langle Z^2 \rangle - \langle Z \rangle^2$ of the Z distribution of the detected fragments are also plotted in terms of positive and negative scattering angles. The linear dependence of σ_Z^2 upon scattering angles is characteristic of diffusion.

Deep inelastic and quasielastic reactions are expected to be limited to a narrow band of incident partial waves between l_{cr} and l_{gr}. We may define an average incident angular momentum $\langle l_i \rangle$ by

$$\langle l_i \rangle = \frac{2}{3} \frac{l_{gr}^3 - l_{cr}^3}{l_{gr}^2 - l_{cr}^2} \simeq 68\ \hbar . \tag{5}$$

In a case in which only a limited number of partial waves contribute to the reaction, the interaction time τ_{int} can be simply related to the scattering angle θ through the equation

$$\tau_{int} = \frac{\theta_{gr} - \theta}{\omega} , \tag{6}$$

where θ_{gr} is the grazing angle and ω is the angular velocity of the dinuclear complex formed during the collision. We determine ω assuming rigid rotation of the dinuclear complex through the equation

$$\omega = \frac{\langle l_i \rangle}{\mathcal{I}} \hbar , \tag{7}$$

where $\mathcal{I}$ is the total moment of inertia of the composite system assuming two tangent rigid spheres

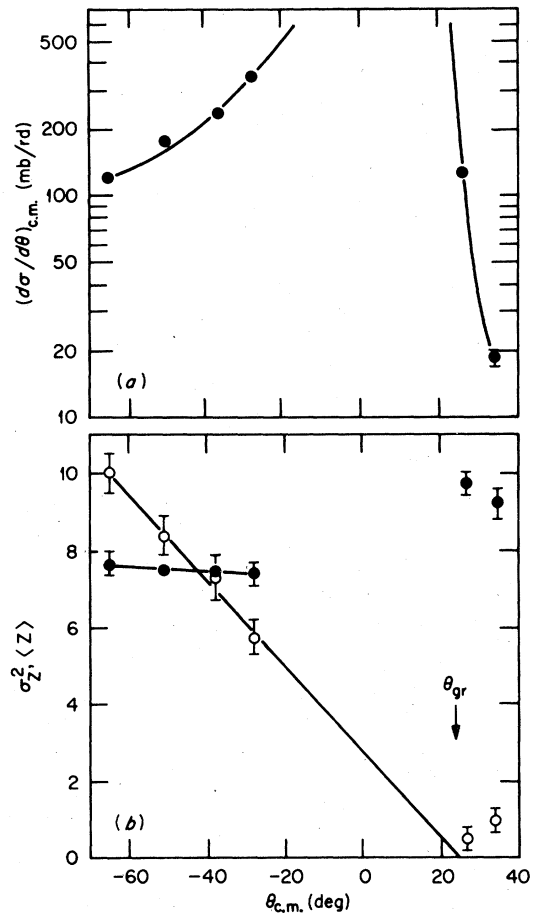

FIG. 6. (a) The differential cross section summed over all reaction products expressed as a function of the c.m. deflection angle. The deeply inelastic component has been associated with negative scattering angles and the quasielastic component with positive angles. (b) Average $\langle Z \rangle$ (solid dots) and variance σ_Z^2 (open circles) of the laboratory Z distributions for positive and negative scattering angles. The lines through the data points are to guide the eye.

with a radius parameter $r_0 = 1.4$ fm. We obtain $\omega = 1.83 \times 10^{21}$ s^{-1}. Having thus defined a time scale for the reaction through Eqs. (6) and (7), it is possible to deduce relaxation times and mass transport coefficients from the experimental data.

We express the mean energy loss ΔE, as a function of the interaction time by

$$\Delta E = \Delta E_0 [1 - \exp(-\tau_{\text{int}} / \tau_R)], \tag{8}$$

where ΔE_0 is the energy loss for complete damping and τ_R is an effective relaxation time for energy dissipation. Dissipation of radial and tangential kinetic energy, as well as energy deformation due to change in shape of the dinuclear complex during the interaction time, contribute to the energy loss ΔE. Thus, the present definition of τ_R is different from that of Ref. 47, where τ_R is defined as the relaxation time for the radial part of the kinetic energy only. A mean experimental energy loss at each angle may be defined by

$$\Delta E(\theta) = \frac{\sum_Z \langle Q^*(\theta, Z) \rangle \left(\frac{d\sigma}{d\theta}\right)_Z}{\sum_Z \left(\frac{d\sigma}{d\theta}\right)_Z}. \tag{9}$$

A fit of the experimental energy loss [defined by Eq. (9)] with Eq. (8) yields a relaxation time $\tau_R = (0.26 \pm 0.04) \times 10^{-21}$ s.

Using a Fokker-Planck equation, with constant charge transport coefficients, Nörenberg *et al.*[8,47] obtain a solution of the charge transport equation which is a Gaussian with mean value

$$\langle Z^* \rangle = Z_p + v_Z \tau_{\text{int}} \tag{10}$$

and variance

$$\sigma_{Z^*}^2 = 2 D_{ZZ} \tau_{\text{int}} , \tag{11}$$

where Z_p is the projectile atomic number and v_Z and D_{ZZ} are the drift and diffusion coefficients for charge, respectively. Assuming that the interaction time τ_{int} is related to the scattering angle θ through Eq. (6), the quantities $\langle Z^* \rangle$ and $\sigma_{Z^*}^2$ should be linear functions of the scattering angle θ. Such a linear dependence is verified by the results shown in Fig. 6(b) and can be used to determine the charge transport coefficients. [The slopes of the lines in Fig. 6(b) are not strongly affected by particle evaporation.] From the slope of the σ_Z^2 vs θ curve, we obtain $D_{ZZ} = (0.58 \pm 0.11) 10^{22}$ (charge units)^2 s^{-1}. This value can be compared to the prediction of the single-particle model of Refs. 48 and 49, which provide analytic expressions for the mass transport coefficients. From Ref. 49 (with their notation), the dynamical set of parameters entering in the calculation of the single-particle transition matrix elements relevant to the present case are $\gamma = 3$ MeV (a fixed parameter), $\Delta j = 3.13\,\hbar$ [Eq. (4.52) of Ref. 49], and $\Delta = 3.79$ MeV [Eq. (4.53) or (4.54) of Ref. 49]. These values, together with a local excitation energy $E^* = 57.9$ MeV yield $D_{AA} = 2.92 \times 10^{22}$ (mass units)^2 s^{-1} for the mass diffusion coefficient. Assuming complete correlation for the transfer of neutrons and protons, the charge diffusion coefficient is given by $D_{ZZ} = (Z/A)^2 D_{AA} = 0.64 \times 10^{-22}$ (charge units)^2 s^{-1}, where Z and A are, respectively, the atomic and mass number of the compound nucleus. This value of D_{ZZ} is in good agreement with the experimental value.

It may be seen from the small slope of the curve $\langle Z \rangle$ vs θ in Fig. 6(b) that the drift coefficient V_Z is extremely small and, in fact, cannot be deduced with precision from our experimental data. This

small value may be understood from the expression given in Ref. 48 for the mass drift coefficient. This coefficient is proportional to the driving force $\partial U_l(A_1)/\partial A_1$. At the injection point the potential energy $U_l(A_1)$ of the composite system presents, for $l > l_{cr}$, a broad maximum, yielding a very weak driving force toward larger mass asymmetry.

B. Gamma-ray results

1. Average γ-ray energies and angular correlations

The γ-ray spectra from NaI detectors 1, 2, 5, and 9 (see Table I) obtained in coincidence with the heavy-ion telescopes were used to determine the average γ-ray energy and angular distributions as a function of the charge, energy, and scattering angle of the fragments.

Typical spectra are shown in Fig. 7 for γ rays in coincidence with (A) evaporation residues detected at $\theta_{lab} = 20°$ and (B) all fragments with $3 \leq Z \leq 16$ detected at $\theta_{lab} = 45°$. Note the enhancement of the yield in the lower energy ($\lesssim 2.2$ MeV) portion of spectrum A. This has been attributed, in the case of heavier nuclei,[50] to collective stretched $E2$ enhancement is also apparent in the case of deep inelastic scattering (spectrum B).

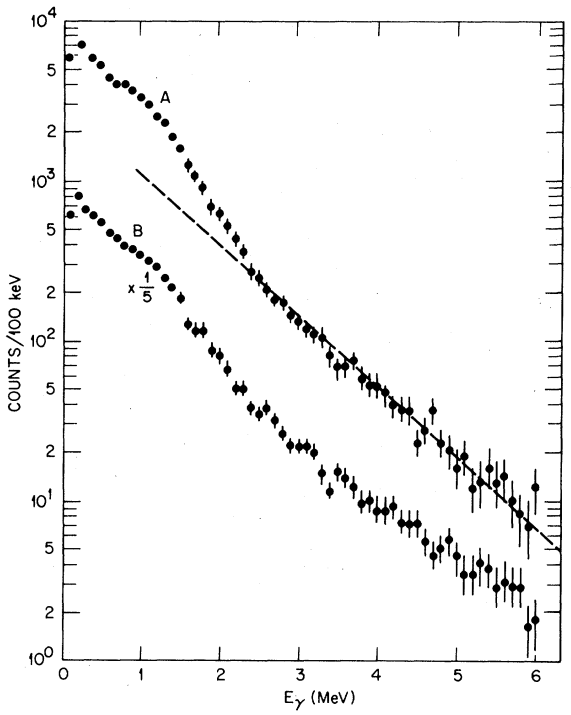

FIG. 7. Gamma-ray spectra obtained in coincidence with (A) evaporation residues at $\theta_{lab} = 20°$ and (B) deep inelastic products with $3 \leq Z \leq 16$ at $\theta_{lab} = 45°$. The NaI detector (NaI-1 in Table I) was located in the reaction plane at an angle of 125° to the beam. The dashed line is an extrapolation of the high energy continuum to lower energies in order to illustrate the enhanced yield of γ rays at energies $\lesssim 2.2$ MeV.

Average γ-ray energies were deduced from the raw spectra by using a slightly modified version of the unfolding technique used by Mollenauer.[51] A set of response matrices consisting of spectra at energy intervals of 100 keV and extending up to 8 MeV was generated for each detector separately by interpolation from spectra obtained in a geometrical configuration reproducing as closely as possible the experimental conditions. Monoenergetic sources and transitions from the low-lying excited states in ^{12}C and ^{16}O populated by inelastic scattering of α particles were used to generate the calibration spectra.

It was found that the average γ-ray energy, $\langle E_\gamma \rangle = (1.8 \pm 0.2)$ MeV, is rather independent of the scattering angle and of the energy of the detected projectile-like fragment, at least for energy losses greater than 35 MeV. There appears to be a slight dependence of $\langle E_\gamma \rangle$ on Z; the average γ-ray energy is 2.0 MeV for the observed products with $Z = 6$, 7, and 8. This slight increase is probably attributable to the high energy γ-ray transitions in ^{12}C, ^{14}N, and ^{16}O, which are seen in the γ spectra.

In order to obtain the in-plane, out-of-plane γ-ray angular correlations, the relative efficiencies of the NaI detectors were carefully checked *in situ* before and after the experiment. The NaI detectors used for this purpose were chosen for their near-identical response as a function of γ-ray energy. In order to eliminate possible effects from scattering on the lead shield, only γ rays above 300 keV were considered. Figure 8 shows the in-plane out-of-plane γ-ray angular distributions obtained for projectile-like fragments with $3 \leq Z \leq 14$ detected at 26° and at 45°. In order to eliminate any contribution from the quasielastic component at 26° for fragments with $7 \leq Z \leq 11$, only those events corresponding to an energy loss greater than 40 MeV were included to get the associated γ yields. For other products at 26° and for all produces at 45°, fragments of all energies could be used. Figure 9 shows the γ-ray angular correlation obtained for evaporation residues detected at 26°.

The out-of-plane anisotropy A is defined here by

$$A = \frac{W(90°) - W(0°)}{W(0°) + W(90°)}, \tag{12}$$

where $W(0°)$ and $W(90°)$ are the γ yields perpendicular to and in the reaction plane, respectively. Figure 8 shows that A is weak ($\lesssim 10\%$). For a product of a given Z, the anisotropy seems independent of scattering angle (it should be noted here

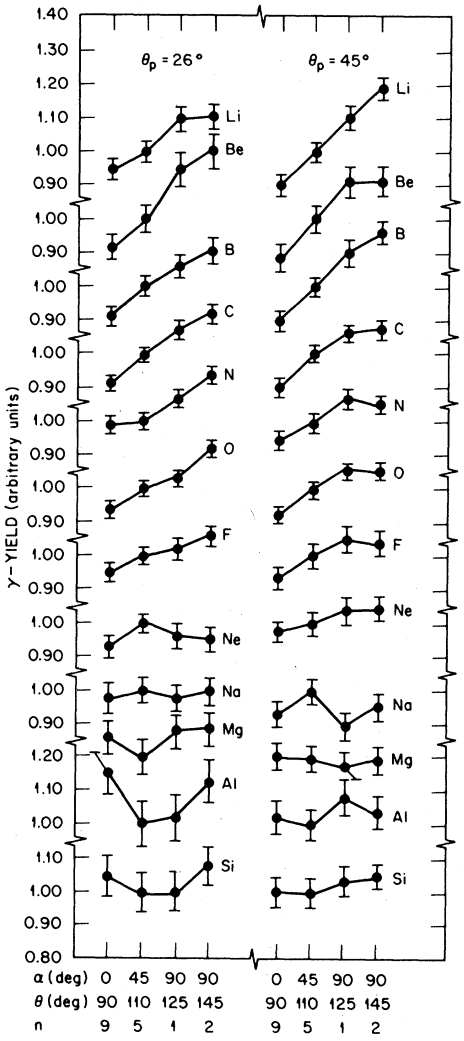

FIG. 8. The in-plane, out-of-plane angular correlations for γ rays detected in coincidence with products at 26° and at 45° having Z values between 3 and 14. The angles α and θ denote the polar angles of the NaI detector with respect to the direction normal to the reaction plane and to the beam, respectively. The integer n is the number of the NaI detector in Table I.

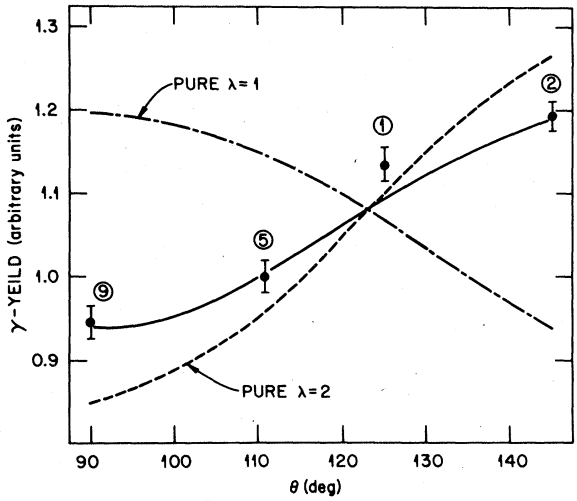

FIG. 9. The angular correlation for γ rays in coincidence with evaporation residues detected at $\theta_{lab}=20°$. The angle θ is the polar angle with respect to the beam and the circled integer denotes the number of the NaI detector as given in Table I. The full curve is the angular correlation expected for a mixture of 25% $\lambda=1$ and 75% $\lambda=2$ stretched transitions.

that only the deeply inelastic component of the particle energy spectra was taken into consideration). The anisotropy decreases with increasing Z of the projectile-like fragment. The in-plane angular correlations were found to be essentially isotropic, although a slight tendency for a higher yield in the direction of the detected fragment was apparent.

These results contrast sharply with what is expected on the basis of the classical picture of angular momentum transfer in strongly damped collisions, viz. a complete alignment of the fragment perpendicular to the reaction plane. If we assume complete alignment and stretched γ-ray transitions, the out-of-plane angular distributions are given by

$$W(\alpha)=\tfrac{5}{4}(1-\cos^4\alpha)\,, \tag{13}$$

for quadrupole transitions and

$$W(\alpha)=\tfrac{3}{4}(1+\cos^2\alpha)\,, \tag{14}$$

for dipole transitions.[30] Here we have taken the perpendicular to the reaction plane as the quantization axis; α is the polar angle with respect to this axis. Thus in the hypothesis of complete alignment and stretched transitions, a 50–65% dipole admixture would be needed to reproduce the measured anisotropy. It seems, from studies of the deexcitation of compound nuclei formed at high excitation energy and angular momentum, that such a high dipole admixture is unlikely.[52,53] Furthermore, even if such an admixture reproduces the observed anisotropy, it fails to reproduce the measured three-point angular correlations of Fig. 8. Thus, the hypothesis of full alignment must be abandoned. We will return to this when we discuss in Sec. IV C a possible source for this lack of alignment.

We consider next the γ-ray angular distribution measured for the evaporation residues. With the beam direction as the axis of quantization, the compound nucleus ^{83}Y is aligned perpendicular to the beam axis. Relative to this axis and in the limit of high spins, the γ-ray angular distribution is expected to be of the form

$$W(\theta)=\tfrac{5}{4}(1-\tfrac{3}{8}\sin^4\theta) \tag{15}$$

for stretched quadrupole transitions and

$$W(\theta) = \tfrac{3}{8}(2 + \sin^2\theta) \qquad (16)$$

for stretched dipole transitions.

The four NaI detectors were located at polar angles $\theta = 90°$, 110.3°, 125.0°, and 145° with respect to the beam axis. The experimental angular distribution (Fig. 9, solid circles) is well described by a 75% quadrupole and 25% dipole mixture (full curve). In this calculation, a small loss of alignment due to particle evaporation has been taken into account according to the method described in Sec. IV B. The symmetry around the beam axis is broken by the detection of the evaporation residues at $\theta_{lab} = 20°$, but this can be neglected; detection of the residues at different angles (10°, 15°, 20°, and 28°) yields identical γ-ray angular correlations, which indicates that this effect is quite small.

Thus, in contrast to the 50–65% dipole admixture which would be necessary to reproduce the γ-ray anisotropy measured for strongly damped collisions, a 25% dipole admixture is quite sufficient to reproduce the anisotropy observed for the evaporation residues. This is further evidence that the small observed γ-ray anisotropy in the case of strongly damped collisions does not have its origin in a very large ($\geq 50\%$) dipole admixture in the γ-ray transitions.

2. *Gamma-ray multiplicity results*

For a given Z of the projectile-like fragment, five energy spectra were generated, corresponding to zero to four fold and higher order coincidences between one heavy-ion telescope and the surrounding NaI detectors. These particle spectra were then divided into energy bins wide enough (10 MeV) to ensure sufficient statistics. For a given energy bin, we make use of the yields in the different fold spectra to determine the first three moments of the γ-ray distribution. If we denote the average γ-ray multiplicity by $\bar{M}_\gamma$, then the width σ_γ os the distribution is defined by the relation $\sigma_\gamma^2 = \langle (M_\gamma - \bar{M}_\gamma)^2 \rangle$ and its skewness by the relation

$$s_\gamma = \frac{\langle (M_\gamma - \bar{M}_\gamma)^3 \rangle}{\sigma_\gamma^3} .$$

A general description of the formalism used to extract the first three moments of the γ-ray multiplicity distribution from the experimental data, which takes into account the effect of neutron detection, γ-ray anistropy, and random coincidences, has been presented in detail elsewhere.[33] The overall effect of neutron detection by the NaI detectors on the first three moments of the γ-ray multiplicity distribution was estimated to be smaller than 10%. Subsequently, this effect was neglected. The γ-ray angular distributions are nearly isotropic and the small measured anistropies have negligible effects on the multiplicity results.

As the deexcitation of compound nuclei has been the object of numerous studies and is relatively well understood, we discuss first the γ-ray multiplicity results for the decay of the compound nucleus ^{83}Y. These data constitute a good basis on which to evaluate the results obtained for strongly damped collisions which will be presented thereafter.

a. Evaporation residues. The three first moments and the relative width $\sigma_\gamma/\bar{M}_\gamma$ of the multiplicity distribution of the γ rays accompanying the deexcitation of the evaporation residues are presented in Table II as a function of the detection angle of the residues. These results represent an average over the energies as well as over masses of the residues (the charges of the individual products were not resolved). Within the limit of the experimental errors, the width and the skewness are independent of detection angle. The average multiplicity, however, decreases smoothly with increasing angle. This trend can be explained qualitatively if the effect of light-particle emission is taken into consideration. The initial recoil direction of the compound nuclei is directed along the beam axis. Only evaporation residues which have received a transverse momentum by particle emission can be detected at an angle different from 0°. The more the evaporation residues deviate from 0°, the larger the transverse momentum they received, and the more massive or energetic, on the average, must be the light particles emitted. In either case, these light particles will tend to carry away a larger fraction of the angular momentum imparted to the compound nucleus, decreasing the number of γ rays necessary to dissipate the remaining angular momentum.

TABLE II. Average $\bar{M}_\gamma$, width σ_γ, skewness s_γ, and relative width $\sigma_\gamma/\bar{M}_\gamma$ of the multiplicity distributions of the γ rays accompanying the evaporation residues formed in the reaction ^{20}Ne + ^{63}Cu, detected at different angles. The last line refers to those quantities averaged over detection angle. The indicated errors are statistical only.

Theta	$\bar{M}_\gamma$	σ_γ	s_γ	$\sigma_\gamma/\bar{M}_\gamma$
10°	11.38±0.04	3.65±0.10	−0.9±0.3	0.32±0.01
15°	11.17±0.05	3.24±0.14	−1.1±0.4	0.29±0.01
20°	10.93±0.05	3.41±0.24	−0.8±0.4	0.31±0.02
28°	10.64±0.07	3.52±0.15	−0.7±0.4	0.33±0.02
Average	11.41±0.05	3.44±0.15	−0.8±0.3	0.30±0.02

In order to define an overall γ-ray multiplicity distribution for the evaporation residues, the moments were weighted by the differential cross section and were then averaged over detection angle. These averaged moments are listed at the end of Table II.

b. Deeply inelastic and quasielastic collisions. The main features of the multiplicity distributions are illustrated in Figs. 10–13. In Fig. 10 the dependence of $\bar{M}_\gamma$ and σ_γ on the energy of the detected particle is compared with the yield of the projectile-like fragments. The dominant features are a general increase in $\bar{M}_\gamma$ as the observed energy decreases (or as the energy loss increases). A maximum is then reached in the region of the deep inelastic peak, after which $\bar{M}_\gamma$ decreases again with further increases in the kinetic energy lost in the collision. Except in the region of very small energy loss, σ_γ is nearly independent of energy loss.

The counting statistics in the 10-MeV-wide energy bins used to determine $\bar{M}_\gamma$ and σ_γ were generally insufficient to determine the skewness with good precision. For the products with the best statistics, the following trends were observed: for small E_{loss}, s_γ is about 2.5. It then decreases to 0 for $E_{\text{loss}} \simeq 40$ MeV, and continues to decrease to a minimum of $\simeq -1.6$ for $E_{\text{loss}} \simeq 70$ MeV. Above this point s_γ increases again to reach a value of $\simeq -0.5$ for $E_{\text{loss}} = 100$ MeV. The dependence of $\bar{M}_\gamma$ on the Z of the detected particle is shown in Figs. 11 and 12 for varying degrees of energy loss. The multiplicity increases with increasing charge asymmetry (i.e., with smaller Z). This Z dependence increases with energy loss. For a given Z and energy loss, $\bar{M}_\gamma$ is not strongly dependent on the scattering angle. Figure 13 presents values of $\bar{M}_\gamma$, σ_γ, and s_γ obtained for a 30-MeV-wide energy bin centered at the maximum of the deep inelastic yield at $\theta_{\text{lab}} = 45°$. The width shows small oscillations as a function of Z around a value of $\simeq 4$. The skewness tends to increase with Z from ~−1.5 to ~0. Essentially identical results were obtained at the other scattering angles.

Several of the above features of the γ-multiplicity results can be understood on the basis of a classical model and the assumption that $\bar{M}_\gamma$ is proportional to the transferred angular momentum. We discuss these features first and then deal with the more unusual aspects of the data.

Classically, the conversion of orbital angular momentum in the entrance channel into intrinsic angular momentum of the fragments is described as the result of tangential frictional forces acting between the fragments.[54] In a first step, the nuclei (assumed spherical) slide on each other generating, under the action of viscous forces,

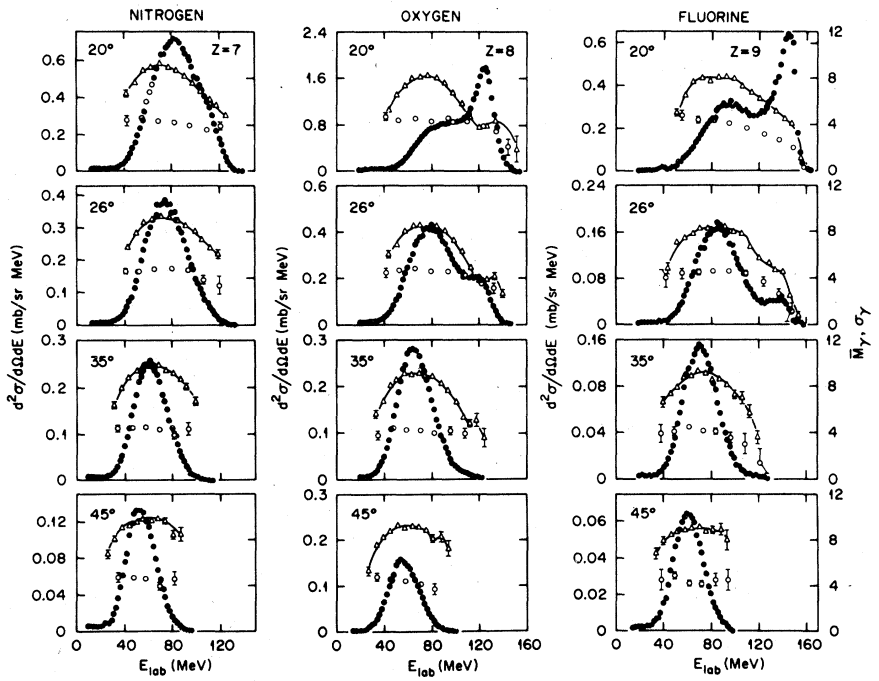

FIG. 10. Values of the average multiplicity $\bar{M}_\gamma$ (triangles) and width of the multiplicity distribution, σ_γ (open circles), as a function of energy of the detected particle for $Z = 7$, 8, and 9 and for $\theta_{\text{lab}} = 20°$, 26°, 35°, and 45°. The singles differential cross section for the fragment yield (solid circles) is also shown. The lines are to guide the eye.

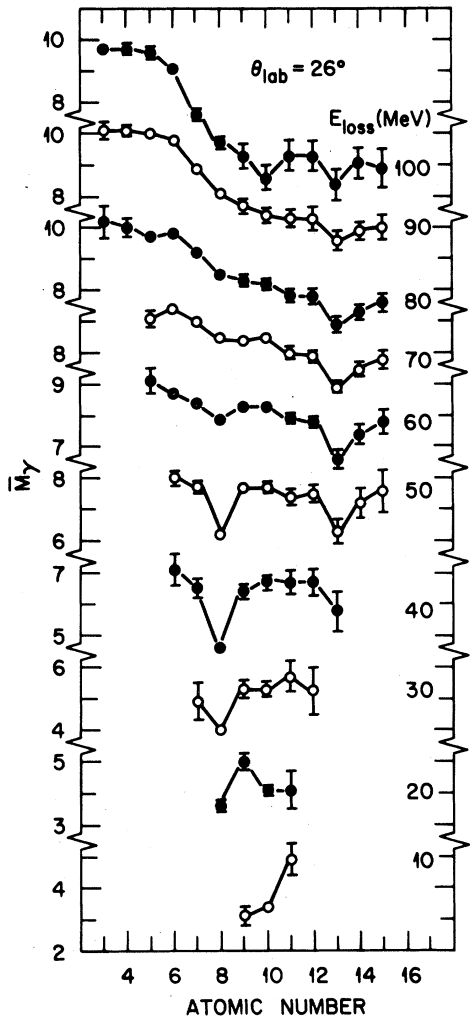

FIG. 11. The multiplicity as a function of the Z of the detected particle for 10-MeV-wide energy-loss bins. The energy loss has not been corrected for the effects of particle emission by the projectile-like fragment. The particles were observed at $\theta_{lab}=26°$.

a torque which sets them into rotation. Tangential fricitional forces continue to act until the system reaches the rolling stage in which the peripheral velocities of the nculei are matched. At this point rolling friction slows down the rotation of the nuclei until they form a rigid body (sticking condition). According to this description of angular momentum transfer, one expects a rapid increase with interaction time (or energy loss), of the angular momentum J transferred to the fragments, until the rolling state is reached. At this point,

$$J=\tfrac{2}{7}l_i\,, \tag{17}$$

where l_i is the incident orbital angular momentum, independent of the mass of the fragments. Then J will continue to increase until it reaches its maximum value at the sticking point, where

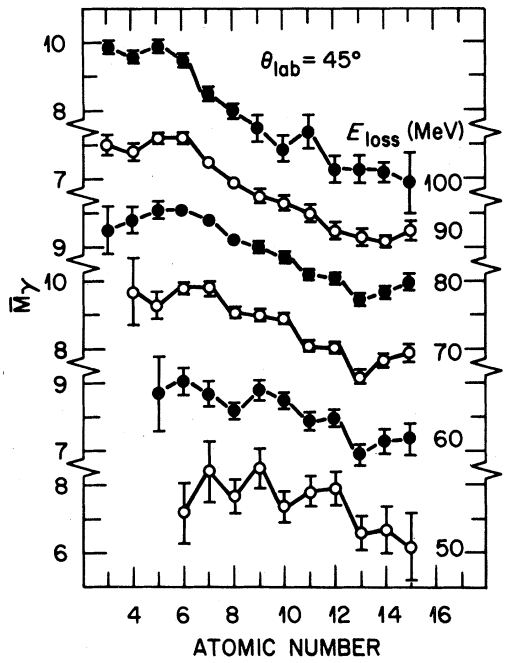

FIG. 12. Same as Fig. 11, except that the particles were observed at 45°.

$$J=\frac{\mathcal{I}_1+\mathcal{I}_2}{\mathcal{I}_1+\mathcal{I}_2+\mathcal{I}_{rel}}\,l_i\,, \tag{18}$$

with $\mathcal{I}_1$ and $\mathcal{I}_2$, the moments of inertia of the fragments and $\mathcal{I}_{rel}$ the moment of inertia associated with relative motion. For a symmetric mass split, the rolling and the sticking stages are equivalent and yield the same value of J. From Eq. 18, one expects J to increase as the mass

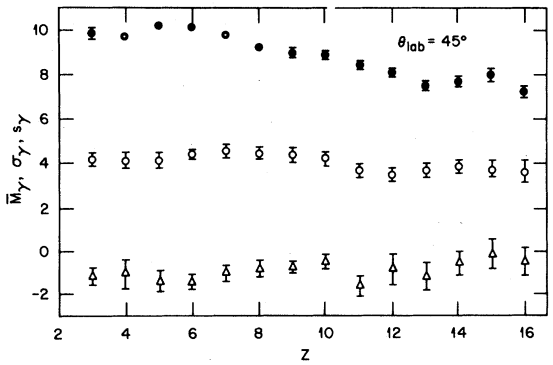

FIG. 13. Average multiplicity (solid points), multiplicity width (open circles), and skewness (triangles) of the γ-ray multiplicity distributions determined for a 30-MeV-wide region of energy covering the maximum of the deep inelastic component of the particle spectrum. These values are given as a function of the Z of the fragment detected at $\theta=45°$.

split of the dinuclear complex becomes more and more asymmetric, leading eventually to complete fusion. The observed increase of multiplicity with increasing energy loss and with increasing mass asymmetry is consistent with this classical picture, and indeed forms the main justification for it.

An interesting behavior of $\bar{M}_\gamma$ is found in the quasielastic region (see Fig. 10). $\bar{M}_\gamma$ first increases rapidly with the energy loss and, after an energy loss of about 15 MeV, shows an abrupt change of slope. At this point, $\bar{M}_\gamma$ seems to reach a plateau and, for the $Z=8$ products, it even displays a minimum near the maximum of the quasielastic yield (Fig. 10). Although several mechanisms can be invoked to explain this behavior,[55] the following one seems most probable. Above $E_{\text{loss}}=15$ MeV, the excitation energy of the fragments becomes sufficient to enable particle emission which then completes with γ-ray emission in the removal of angular momentum.

As the energy loss continues to increase, $\bar{M}_\gamma$ starts to increase again to reach a broad maximum over the deeply inelastic component. For increasing energy loss, however, $\bar{M}_\gamma$ decreases rapidly. Although such a drop in $\bar{M}_\gamma$ has been noticed previously,[24] it has drawn little attention or it has been dismissed as resulting from the presence of light contaminants on the target. Indeed, fusion with contaminants like carbon or oxygen would produce evaporation residues with low kinetic energies and with atomic numbers similar to the projectile-like fragments. Measurements with a carbon target in the same experimental condition yield $\bar{M}_\gamma=1$ to 2. The drop in $\bar{M}_\gamma$ happens for an energy loss where the yield of the projectile fragment decreases rapidly, which renders the contaminant problem even more critical. Thus, a small amount of carbon or oxygen contaminant could cause the drop in the measured γ-ray multiplicity. By close comparison between the spectra obtained with the ^{63}Cu and natural carbon targets, it was estimated that the amount of light contaminants did not exceed 1 μg/cm^2 at the end of each run and that this could not be responsible for the observed drop in $\bar{M}_\gamma$. Furthermore, the decrease in $\bar{M}_\gamma$ is observed for silicon, phosphorous, and sulfur products detected at 45° and these are not residues of the fusion of Ne+C or Ne+O.

Several mechanisms can be invoked to explain this decrease in $\bar{M}_\gamma$. (i) The decrease happens for very large energy losses which translate into high excitation energy of the fragments. These then deexcite by emission of a large number of light particles carrying a larger fraction of the transferred angular momentum. This possibility will be discussed further in Sec. IV. (ii) The fragments emerge with a kinetic energy well below the kinetic energy expected from the repulsion of spherical fragments, which implies strong deformation at scission. By inspection of Eq. (18), one may see that a large increase in the relative moment of inertia leads to a decrease in the transferred angular momentum. It is, of course, possible that both mechanisms contribute to the observed decrease in $\bar{M}_\gamma$.

The value of $\bar{M}_\gamma$ obtained for oxygen ions of energy loss less than 60 MeV seems anomalously low (see Fig. 11). This effect is most pronounced at forward angles (20°, 26°) and nearly disappears at larger angles such as 45° (Fig. 12). Although the origin of this minimum is not yet completely clear, it is possible that the oxygen yield at forward angles and for smaller Q values (i) contains a large component of a quasielastic reaction in which an excited ^{20}Ne decays by α emission to the ground state of ^{16}O and/or (ii) results from the direct breakup of ^{20}Ne into $^{16}\text{O}+\alpha$. A more quantitative interpretation of the results requires the deduction of the transferred angular momentum from the measured γ-ray multiplicity; this is discussed in the next section.

IV. DISCUSSION

A. Conversion of gamma-ray multiplicity to angular momentum

The γ-ray multiplicity includes contributions from both the light and the heavy fragments but is independent of the relative orientation of their respective angular momenta, $\vec{J}_L$ and $\vec{J}_H$. Thus, $\bar{M}_\gamma$ depends on the average angular momentum $\langle J\rangle=\langle|\vec{J}_L|+|\vec{J}_H|\rangle$.

For reactions between much heavier nuclei, it is generally assumed[17,20,21] that the fragments deexcite in two steps. First, emission of light particles (mainly neutrons) occurs with little dissipation of angular momentum until the residual excitation becomes small enough to permit γ-ray competition. At this stage, a cascade of γ rays is emitted including a few statistical γ rays removing on the average rather little angular momentum and a large number of stretched $E2$ transitions which are responsible for most of the angular momentum dissipation. In such a case, the average angular momentum $\langle J\rangle$ of the fragments can be related to the multiplicity $\bar{M}_\gamma$ through the simple equation,

$$\langle J\rangle=2(\bar{M}_\gamma-k)\,, \tag{19}$$

where k is the number of statistical transitions. In fact, recent studies[56] have shown, even in the case of heavy fragments, that strong effects of the

internal structure of the nuclei on the multipole composition of the emitted γ ray can cause the relation between angular momentum and γ-ray multiplicity to be more involved than previously assumed. For lighter systems, such as the present one, it is obvious by comparing our multiplicity results on the decay of the compound nucleus ^{83}Y with the average initial angular momenmentum deduced from the fusion cross section, that Eq. (19) is inadequate. Assuming a triangular J distribution up to l_{cr} in the compound nucleus ^{83}Y, one deduces an average angular momentum $\langle J\rangle = \frac{2}{3} l_{cr} = 40\ \hbar$. However, only 11.4 γ rays (see Table II) are emitted on average by the evaporation residues. Even if all the transitions were stretched $E2$, which is an unrealistic assumption for these nuclei, Eq. (19) would allow a maximum of 23.8 $\hbar$ to be dissipated by γ-ray emission. Thus, contrary to the situation for heavier systems, a large fraction of the angular momentum must be dissipated by light-particle emission.

Using available experimental information[52,57-60] on the decay of compound nuclei in the mass 60 region, we have derived an empirical relation between the multiplicity and the transferred angular momentum. The information consists of experiments in which l_{cr} and $\bar{M}_\gamma$ have been determined independently over a large range of excitation energy, 30 MeV $\leq E_x \leq$ 120 MeV, and for a variety of projectile and target combinations, i.e., for different combinations of angular momentum distribution and excitation energy. This leads to the following empirical equation:

$$\langle J\rangle = \langle J_0\rangle + \tfrac{3}{16}(E^* - E_0) + 2(\bar{M}_\gamma - k)\,, \qquad (20)$$

with $\langle J_0\rangle = (11-12)\ \hbar$ and $E_0 = 80$ MeV. In this expression, the first two terms represent the average angular momentum removed by particle emission as a function of the effective excitation energy E^* deduced from Fig. 3(b). Thus for an excitation energy of 80 MeV, which is comparable with the Q values measured here for fully damped products, the angular momentum removed by particle emission is 11 to 12 $\hbar$. In agreement with Albrecht *et al.*[12] we find that, for a 16 MeV increase in excitation energy, an extra 3 $\hbar$ of angular momentum is removed by particle emission. The last term represents the average angular momentum dissipated by the γ rays, assuming $\bar{M}_\gamma - k$ stretched $E2$ transitions and k statistical γ rays. From a study of the fusion of ^{16}O + ^{58}Ni, Simpson *et al.*[52] have adopted the value $k = 2$.

Although Eq. (20) does not contain any explicit dependence of particle emission upon the initial angular momentum, it reproduces quite well a large variety of experimental data. In particular, using the multiplicity data of Geoffroy *et al.*[59,60] on the decay of the compound nuclei ^{39}K and ^{70}Se for formed in the reactions ^{12}C + ^{27}Al and ^{12}C + ^{58}Ni, it reproduces the dependence on excitation energy of the average angular momentum deduced from the fusion cross sections.

When applied to our results for the decay of the compound nucleus ^{83}Y at 125-MeV excitation energy ($\bar{M}_\gamma = 11.4$), Eq. (20) yields $\langle J\rangle = 39.5\ \hbar$, in excellent agreement with the value 40 $\hbar$ deduced from the fusion cross section. Thus, about 20 $\hbar$ of angular momentum are dissipated by particle emission. Assuming that the width σ_J is related to σ_γ in the same manner that $\langle J\rangle$ is related to $\bar{M}_\gamma$, the J distribution in the residual nuclei prior to γ decay is characterized by $\langle J\rangle = 19 \pm 1\ \hbar$, $\sigma_J = 5.7 \pm 0.4\ \hbar$, and $s_J = -0.8 \pm 0.3$.

In a separate study of the decay of the compound nucleus ^{75}Br formed at an excitation energy of 115 MeV in the bombardment of a ^{63}Cu target with a 133-MeV ^{12}C beam, we obtained a value of $\bar{M}_\gamma = 9.5$. Application of Eq. (20) produces an initial average angular momentum of 33.5 $\hbar$, again in good agreement with the value 31 $\hbar$ deduced from the fusion cross section. In this case, ~18 $\hbar$ are dissipated by particle emission and 15 $\hbar$ by γ rays.

Equation (20) may be used to determine the angular momentum transfer as a function of energy loss and, in this respect, may shed some light on the observed decrease in $\bar{M}_\gamma$ at very large energy losses (cf. Fig. 10). The average transferred angular momentum $\langle J\rangle$ deduced with Eq. (20) is shown in Fig. 14 as a function of the energy loss in the primary collision. The data are at two scattering angles for projectile-like fragments with $Z = 8$ and 9. The energy bins are 10 MeV wide. It may be seen that $\langle J\rangle$ increases with energy loss over nearly the whole range and exhibits only a slight decrease for the largest energy losses. Thus, it appears that most of the drop in the multiplicity at large energy losses can be accounted for on the basis of particle emission. The amount of the remaining decrease in $\langle J\rangle$ near $E_{loss} = 90-100$ MeV is not very large and depends on the accuracy of Eq. (20) over a large range of excitation energy. It is, of course, possible that the dependence of $\langle J\rangle$ on E_{loss} shown in Fig. 14 also reflects the onset of strong deformations in the exit channel at large energy loss.

Application of Eq. (20) to values of $\bar{M}_\gamma$ measured for a 30-MeV-wide energy bin (Fig. 13) covering the deep inelastic peak yields the average transferred angular momentum $\langle J\rangle$ shown as a function of the primary light fragment atomic number Z^* in Fig. 15. Comparing Figs. 13 and 15, we see that the average angular momentum $\langle J\rangle$ depends more strongly on Z^* than does $\bar{M}_\gamma$. This arises

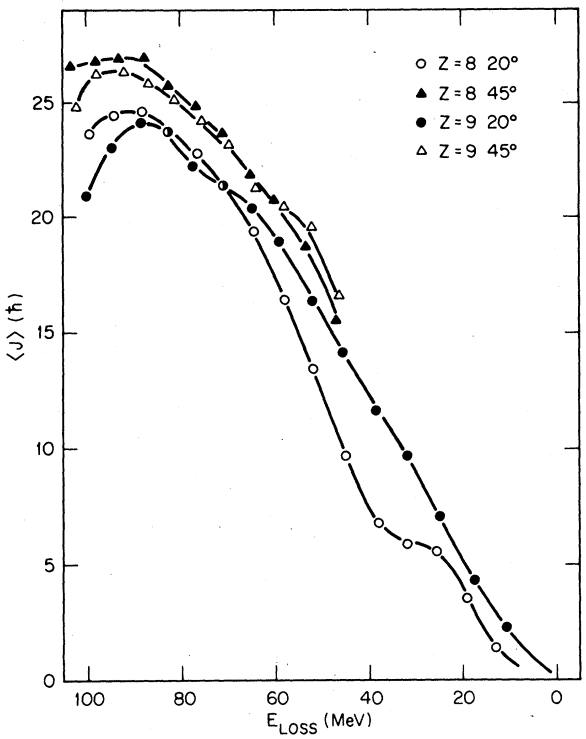

FIG. 14. The transferred angular momentum $\langle J \rangle$, averaged over 10-MeV-wide bins as a function of energy loss for $Z = 8$ and 9 projectile-like fragments detected at different angles. The lines through the data points are to guide the eye.

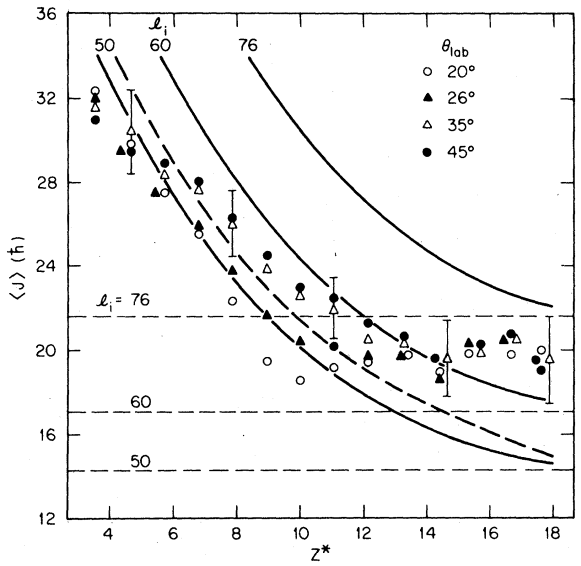

FIG. 15. The angular momentum transferred to the fragments as a function of Z^* of the primary projectile-like fragment. The full curves are obtained in the sticking limit for spherical fragments and different values l_i for the contributing incident partial wave. The light dashed curves correspond to the rolling limit while the heavy dashed curve has been calculated in the sticking hypothesis with deformed fragments (see text) and an average value $\langle l_i \rangle = 68\ \hbar$ for the contributing incident partial waves.

from the correction for particle emission which increases from $\sim\frac{1}{3}$ for the higher Z^* products to $\sim\frac{1}{2}$ for the smaller Z^* products. For the fragments most remote from the projectile, $\langle J \rangle$ is independent of detection angle, whereas for the fragments near the projectile $\langle J \rangle$ first increases with angle, then reaches a constant value at 35° which corresponds to the sticking condition. This limit is also reflected in the energy spectra which are completely relaxed beyond 35°.

For comparison, we have indicated on Fig. 15 the predictions of the rolling and sticking limits given by Eqs. (17) and (18), respectively, assuming spherical fragments and taking three different values for the incident partial waves, $l = l_{gr} = 76\ \hbar$, $l = l_{cr} = 60\ \hbar$, and $l = 50\ \hbar$. At 35° and 45° where the sticking condition should be reached, the experimental points should lie between the curves defined by the grazing and the critical angular momenta. In fact, the partial waves contributing to strongly damped collisions seem to extend from ~68 $\hbar$ for the heavier fragments to less than 50 $\hbar$ (~10 $\hbar$ below l_{cr}) for the lighter fragments. Similar results have been obtained in other light systems.[13,16] If the deformation of the fragments is taken into account, most of the above discrepancies are removed, as shown below and in Ref. 16.

With the assumption of rigid rotation of the dinuclear complex at scission, the total kinetic energy of the fragments can be expressed as the sum of their Coulomb repulsion and rotational energies,

$$E_{K\,\mathrm{c.m.}} = \frac{Z_1 Z_2 e^2}{d} + \frac{l_f(l_f+1)\hbar^2}{2\mu d^2}, \tag{21}$$

where d is the separation distance of the fragments at scission and l_f is their relative orbital angular momentum. Experimentally, $E_{K\,\mathrm{c.m.}} = E_{\mathrm{c.m.}} + Q^*$, where $E_{\mathrm{c.m.}}$ is the incident center-of-mass energy and Q^* the reaction Q value, taking into account the effect of particle emission [Fig. 3(b)]. In the sticking limit, the average orbital angular momentum $\langle l_f \rangle$ is given by

$$\langle l_f \rangle = \langle l_i \rangle - \langle J \rangle, \tag{22}$$

where $\langle l_i \rangle = 68\ \hbar$ is the average incident orbital angular momentum producing a deep inelastic collision and $\langle J \rangle$ is the average angular momentum transferred to the fragments. For $\langle J \rangle$, we used the values deduced from the γ-ray multiplicity measurements for a scattering of 45° where we expect the sticking limit to be reached. Equation (21) was then used to determine the distance d and to divide the total kinetic energy into Coulomb energy

and rotational energy as shown in Fig. 16. The rotational energy varies between 15 and 20 MeV and for light projectile-like fragments is of the same order as the Coulomb energy while it represents about 25% of the total kinetic energy for the heavier fragments.

Assuming a configuration at scission in which the two fragments are approximated by two tangent ellipsoids with their axes of symmetry along the axis joining their center, one deduces from the value of d in Eq. (21) a deformation parameter $\beta \simeq 0.6$. This large deformation is consistent with other experimental determinations.[24,61] Making use of Eq. (18) in which the moments of inertia become those of the deformed fragments, and $\langle l_i \rangle = 68\ \hbar$, the angular momentum transferred to the fragments is given by the dashed curve in Fig. 15. A much improved agreement with the experimental data is obtained for $Z^* = 4$–12, although the experimental values for the heaviest projectile-like fragments now exceed the calculated values. Thus, the inclusion of deformation can bring the magnitude of the transferred angular momentum expected for a narrow band of partial waves (60–70 $\hbar$) and the sticking limit into better agreement with measured multiplicities. Some apparent preference for high partial waves to produce symmetric mass splits still remains (on the basis of Fig. 15 alone).

Following Wolschin[29] and Riedel *et al.*[47] we express the averaged transferred angular momentum as

$$\langle J \rangle = \langle J_0 \rangle \left[1 - \exp\left(-\frac{\mathcal{I}}{\mathcal{I}_{\text{rel}}} \frac{\tau_{\text{int}}}{\tau_I} \right) \right] , \tag{23}$$

where $\langle J_0 \rangle$ is the largest angular momentum transferred, $\mathcal{I}$ and $\mathcal{I}_{\text{rel}}$ are the total and relative moments of inertia, respectively, τ_I is the angular momentum relaxation time, and τ_{int} the interaction time. The average angular momentum transferred for a given scattering angle may be defined experimentally as

$$\langle J \rangle = \frac{\sum_Z \langle J \rangle_Z \left(\frac{d\sigma}{d\theta} \right)_Z}{\sum_Z \left(\frac{d\sigma}{d\theta} \right)_Z} , \tag{24}$$

where $\langle J \rangle_Z$ and $(d\sigma/d\theta)_Z$ are the average angular momentum and the differential cross section measured for a particular Z of the projectile-like fragment. By fitting the average transferred angular momentum thus determined with Eq. (23) in which the interaction time τ_{int} has been related to the scattering angle through Eqs. (6) and (7), we deduce an angular momentum relaxation time $\tau_I = 0.41 \pm 0.06 \times 10^{-21}$ s. This time is about twice as long as the energy relaxation time. With the same set of parameters as in Sec. III A 3, the single-particle model of Refs. 48 and 49 yields $D_{MM} = 7.2 \times 10^{22}\ \text{s}^{-1}$ for the angular momentum diffusion coefficient, leading to a relaxation time $\tau_I = 0.53 \times 10^{-21}$ s in fair agreement with the experimental result.

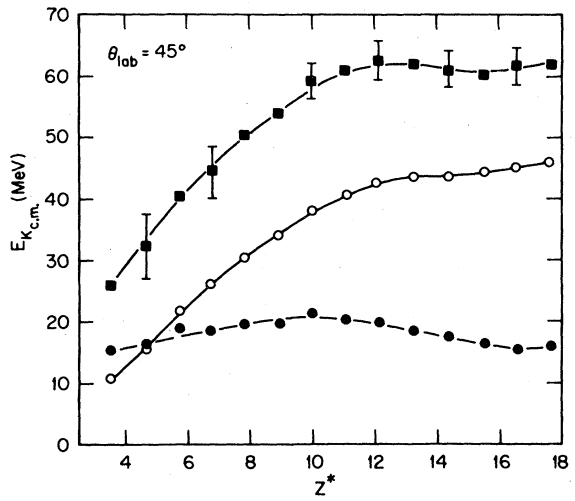

FIG. 16. The total center-of-mass kinetic energy (squares), the Coulomb repulsion energy (open circles), and rotational energy (solid circles) as a function of the Z^* of the primary projectile-like fragment. The calculation of the Coulomb and rotational energies includes deformation of the fragments, as described in the text.

B. Effects of particle evaporation

In the previous section, we have seen how light particle emission plays an important role in angular momentum dissipation. We next consider how it affects the alignment and distribution of the angular momenta of the fragments prior to γ-ray emission.

1. Evaporation residues

In first approximation, the relative width $\sigma_J/\langle J \rangle$ and the skewness s_J define the shape of the J distributions. Assuming a triangular J distribution up to l_{cr} in the compound nucleus, the first moments are given by $\langle J \rangle = \frac{2}{3} l_{\text{cr}} = 40\ \hbar$, $\sigma_J = l_{\text{cr}}/18^{1/2} = 14.1\ \hbar$, and $s_J = -8^{1/2}/5 = -0.57$. The relative width is then defined by $\sigma_J/\langle J \rangle = 8^{-1/2} = 0.35$. These predicted quantities are in excellent agreement with the corresponding experimental quantities $\sigma_\gamma/\bar{M}_\gamma = 0.30 \pm 0.2$ and $s_\gamma = -0.8 \pm 0.3$ obtained for the γ-ray multiplicity distribution. Thus, the effect of particle evaporation is essentially to shift the initial J distribution ($\langle J \rangle = 40\ \hbar$) toward lower J values in the residual nucleus ($\langle J \rangle = 19\ \hbar$), but with little change in shape. Such an effect has been

noticed previously in different studies of the decay of compound nuclei.[20,52,62]

In order to have more detailed information on the effect of particle evaporation, statistical model calculations were performed using the Monte Carlo code JULIAN.[43] In these calculations, the distribution of the partial waves contributing to the reaction cross section was determined from an optical model calculation with parameters deduced from elastic scattering measurements. This distribution was then scaled down in order to obtain a J distribution in the compound nucleus which reproduces the measured fusion cross section (see Fig. 17). Light-particle (p,n,α) transmission coefficients were determined using standatd optical model parameters.[63,64] Standard parameters for the pairing gap and moment of inertia were also used in the level density formula.[65] For γ-ray emission, a retardation factor of ~5 for quadrupole transitions[66] was adopted. It was assumed that the compound nucleus was initially completely aligned in the $M=0$ magnetic substate (here, the quantization axis is the beam axis). The code kept track of the spin orientation after each particle emission so that at the end of the evaporation process not only the J distribution but also the M distribution for each value of J was known for each residual nucleus.

The overall J distribution in the residual nucleus prior to γ decay is shown in Fig. 17. Its three first moments are $\langle J\rangle = 16.2\ \hbar$, $\sigma_J = 5.2\ \hbar$, $s_J = -0.10$ with a relative width $\sigma_J/\langle J\rangle = 0.32$, in fair agreement with the γ-ray multiplicity results (see Sec. IV A). The degree of alignment is described by the quantity $\langle M/J\rangle$ and its variance $\sigma(M/J)$, where M is the projection of J along the beam axis. Starting from a completely aligned compound nucleus [$\langle M/J\rangle = 0$ and $\sigma(M/J) = 0$], the calculation yields $\langle M/J\rangle = 0$ as expected and $\sigma(M/J) = 0.32$, corresponding classically to a spin orientation of $90° \pm 18°$ relative to the beam axis. These J and M distributions were used (see Sec. IV C) to calculate the γ-ray angular correlation shown in Fig. 9 which, for a 25% dipole admixture, is in agreement with the experimental data.

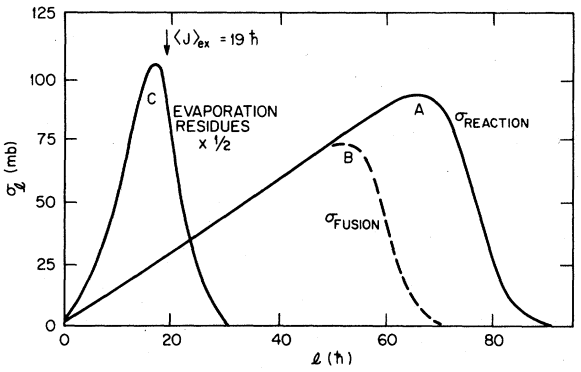

FIG. 17. (A) l distribution deduced from an optical model calculation of the total reaction cross section (σ_{reaction}). (B) l distribution in the compound nucleus after scaling down the previous distribution in order to reproduce the fusion cross section (σ_{fusion}). (C) l distribution in the evaporation residues as calculated with the code JULIAN.

The J distribution after particle emission depends, of course, on the parameters used in the statistical model calculations. It is particularly sensitive to the competition between the different modes of decay. An increase in α competition, for example, leads to a marked decrease in $\langle J\rangle$. To a lesser extent, $\langle J\rangle$ depends also on the γ-ray strength used. However, a decrease in $\langle J\rangle$ is accompanied by an almost proportional decrease in σ_J leaving the relative width $\sigma_J/\langle J\rangle$ unchanged. Similarly, it was found that the calculated skewness and the loss of alignment were very insensitive to the parameters used in the calculation. This point is very important for the analysis of the results for the strongly damped collision.

2. *Strongly damped collisions*

As we have noted earlier, strongly damped collisions are expected to occur within a band of incident partial waves between $l_{cr} = 60\ \hbar$ and $l_{gr} = 76\ \hbar$. In the sharp cutoff approximation, the three first moments and the relative width of the distribution of the contributing partial waves are $\langle l\rangle = 68\ \hbar$, $\sigma_l = 4.5\ \hbar$, $s_l \approx 0$, and $\sigma_l/\langle l\rangle = 0.07$. In the sticking limit, which should be valid for all products at 45°, the angular momentum imparted to the fragments is directly proportional to l [Eq. (18)]. This should hold for fragments having energies near the maximum of the fully relaxed deep inelastic yield. Thus, for a given pair of fragments, assuming that all partial waves between l_{cr} and l_{gr} contribute, one expects a distribution of the transferred angular momentum which is the image of the initial l distribution, i.e., which has the same relative width and skewness. In the absence of particle emission, the γ-ray multiplicity distributions should also have the same shape, $\sigma_\gamma/\bar{M}_\gamma = 0.07$ and $s_\gamma \sim 0$. These values are in sharp disagreement with the experimental data (see Fig. 18). [Note that the experimental data are obtained at $\theta_{\text{lab}} = 45°$ where only fully relaxed events should be present and that only events in a narrow region of energy (±15 MeV) around the most probable energy were used.] The measured values of $\sigma_\gamma/\bar{M}_\gamma = (0.4\text{–}0.5)$ are in fact even larger than for the evaporation residues (for which all partial waves between $l=0$ and l_{cr} participate). This indicates that the above discrepancy does not originate

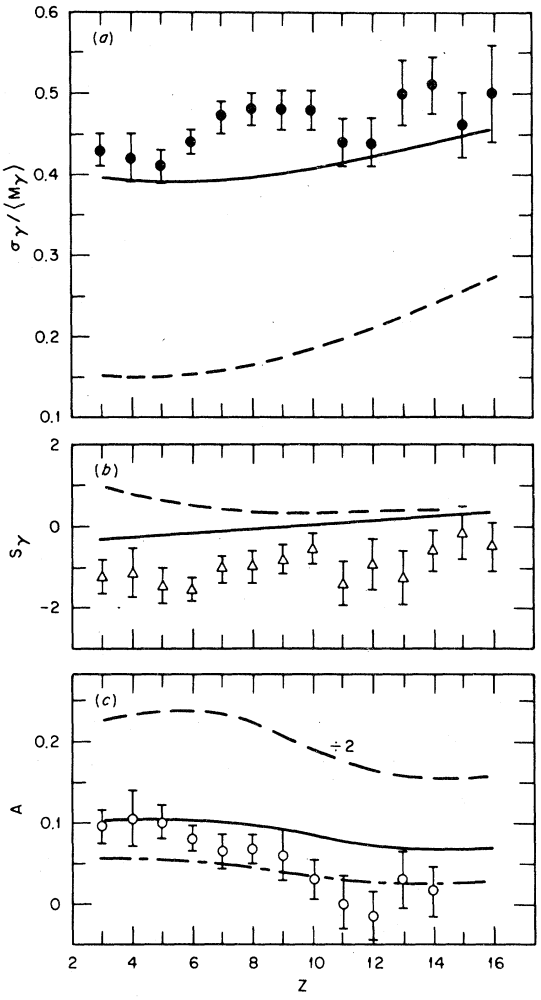

FIG. 18. Properties of the γ-rays associated with the strongly damped collisions: (a) relative width σ_γ/M_γ, (b) skewness s_γ of the multiplicity distribution, and (c) out-of-plane γ-ray anisotropy A. The abscissa is the Z of the projectile-like fragment detected at $\theta_{lab}=45°$ with an energy within ±15 MeV of the most probable energy in deep inelastic component. Predictions assuming complete alignment at scission and including the effects of particle emission are indicated by the dashed curves; the γ-ray anisotropy in (c) was calculated with the assumption of two dipole transitions and was divided by two before plotting. The effect on the predicted value of A of adding a fluctuating component J_f to the aligned component J_0 is illustrated for $\langle J_f\rangle/\langle J_0\rangle = 0.9$ by the solid curve and for $\langle J_f\rangle/\langle J_0\rangle = 1.2$ by the dash-dotted curve. Very similar values of $\sigma_J/\langle J\rangle$ and s_J are predicted for $\langle J_f\rangle/\langle J_0\rangle = 0.9$ and 1.2 and are shown in each case by a single full curve.

with the assumption that only l values between 60 and 76 $\hbar$ are involved.

In order to determine the effect of particle emission an iterative procedure was used with the following initial assumptions: (i) The average angular momentum imparted to the fragments is given by the γ-ray multiplicity measurements (Fig. 15). (ii) The fragments share an amount of excitation energy [Fig. 3(b)] proportional to their masses and an amount of angular momentum proportional to their moments of inertia. (iii) The shape of the J distribution in a fragment is determined by the sharp cutoff approximation and the sticking limit. (iv) The primary fragments are completely aligned in a direction perpendicular to the reaction plane. (v) The fragments have reached equilibrium before particle emission. The code JULIAN was then used to determine the J distribution and the spin alignment of the residual fragments after particle emission. Because of their small sensitivity to the ratio $\sigma_J/\langle J\rangle$, we chose to characterize the calculated J distributions in the residual nuclei by this quantity rather than by the average $\langle J\rangle$ and the width σ_J. The calculated values of $\sigma_J/\langle J\rangle$ and s_J are compared to the experimental data in Figs. 18(a) and 18(b) (dashed lines) as a function of the Z of the projectile-like fragment. Although particle evaporation significantly increases $\sigma_J/\langle J\rangle$ from its initial value of 0.07 to 0.15 for $Z=3$ and to 0.27 for $Z=16$, the result is still smaller than the experimental value by a factor of ~3. The calculated skewness is positive and it decreases with the Z of the projectile-like fragment, again in disagreement with the data. The loss of alignment due to particle emission is characterized by values of $\langle M/J\rangle$ decreasing from 0.98 for $Z=3$ to 0.95 for $Z=16$, which corresponds to depolarization angles of 11.5° and 18.2°, respectively. With the assumption of stretched transitions containing on the average two dipole γ rays (i.e., a 20–30% dipole admixture consistent with the evaporation-residue results), the calculated J and M distributions were used to compute the out-of-plane γ-ray anisotropy shown in Fig. 18(c) by the dashed line. Here again, there is a sharp disagreement with the experimental data (note that the prediction has been divided by a factor of 2 for plotting).

Particle emission and a reasonable dipole admixture thus cannot account for the large width of the multiplicity distribution and the small out-of-plane anisotropy measured for the γ rays. It appears to us that the above discrepancies have their origin in the assumptions made about the reaction mechanism. The assumption of fully aligned fragments is particularly suspect. Figure 18(c) strongly suggests that the alignment of the fragments at scission is incomplete. We will show in the following section that a common explanation of the results of Figs. 18(a)–18(c) can be found if we abandon the hypothesis of full alignment of the fragments at scission.

C. Randomly oriented component of the transferred angular momentum

In order to preserve generality in the interpretation of our experimental results, we propose the following very simple and highly schematic model. It is assumed that the angular momentum J imparted to the fragments can be divided into two components: (i) a component J_0 arising from tangential friction aligned perpendicular to the reaction plane, with a narrow distribution $P(J_0)$ given by the sharp cutoff approximation and the sticking limit ($\sigma_J/\langle J\rangle = 0.07$, $s_J = 0$); (ii) a randomly oriented component J_f, the magnitude of which for simplicity is assumed to be proportional to J_0. Thus, $\vec{J} = \vec{J}_0 + \vec{J}_f$ and $M = M_0 + M_f$. Taking the axis perpendicular to the reaction plane as the quantization axis, the probability $P_J(M)$ to obtain a particular value of J with projection M is given by

$$P_J(M) = \sum_{J_0=J-J_f}^{J+J_f} P(J_0) \times \frac{|\langle J_0, M_0 = J_0, J_f, M_f = M - J_0 | J, M\rangle|^2}{2J_f + 1} \tag{25}$$

and the probability $P(J)$ to obtain a particular value of J is given by summing over all possible values of M:

$$P(J) = \sum_M P_J(M) , \tag{26}$$

where $\langle J_0, M_0 = J_0, J_f, M_f = M - J_0 | J, M\rangle$ is the Clebsch-Gordan coefficient coupling the vectors $|J_0, M_0 = J_0\rangle$ and $|J_f, M_f\rangle$ to give the vector $|J, M\rangle$. The distributions $P(J)$ and $P(J_0)$ satisfy the condition $\sum_J P(J) = \sum_{J_0} P(J_0)$. Thus, in principle, the distributions $P_J(M)$ and $P(J)$ can be calculated from the distribution $P(J_0)$ and then used in the evaporation code to obtain the final J and M distributions. As the calculation must be repeated for each value of the ratio $\langle J_f\rangle/\langle J_0\rangle$, this would be a lengthy and expensive process. In order to shorten the calculation, the coupling of the aligned and random angular momentum was done after the particle evaporation calculation by replacing Eq. (25) with the following expression:

$$P_{J'}(M') = \sum_{J_0'=J'-J_f'}^{J'+J_f'} \sum_{M_0'} P_{J_0'}(M_0') \frac{|\langle J_0', M_0', J_f', M_f' | J', M'\rangle|^2}{2J_f' + 1} . \tag{27}$$

Equation (26) is replaced with

$$P(J') = \sum_{M'} P_{J'}(M') , \tag{28}$$

where the prime refers to quantities taken after particle emission. The probability distributions $P_{J'}(M_0')$ are given by the statistical model calculation as described in the previous section and thus need not be repeated for different values of $\langle J_f\rangle/\langle J_0\rangle$. As the two modes of angular momentum coupling (before and after particle emission) are not equivalent, a simple test case was run using both methods to check for possible effects on the final distributions $P_{J'}(M')$. The two calculations yielded the same distributions to a very good approximation, justifying the use of Eqs. (27) and (28).

For each assumed value of the ratio $\langle J_f\rangle/\langle J_0\rangle$, the distributions $P_{J_H'}(M_H')$ and $P(J_H')$ in the heavy fragments (the index H denotes the heavy fragment) were determined through Eqs. (27) and (28). It was assumed that the distributions $P_{J_L'}(M_L')$ and $P(J_L')$ (the index L denotes the light fragment) could be deduced from their counterpart in the heavy fragment by a simple scaling such that the ratio $\langle J_L'\rangle/\langle J'H\rangle$ is given by the ratio of the moments of inertia of the fragments. Assuming further that the respective orientations of the random component in each fragment are uncorrelated, the distribution $P(J)$ of $J = |\vec{J}_L'| + |\vec{J}_H'|$ (which can be compared directly to the γ-ray multiplicity distribution) is given by

$$P(J) = \sum_{J_L' J_H'} P(J_L') P(J_H') , \tag{29}$$

where the sum over J_L' and J_H' must satisfy the condition $|\vec{J}_L'| + |\vec{J}_H'| = J$. The three first moments of $P(J)$, as well as the relative width $\sigma_J/\langle J\rangle$, were determined for each assumed value of the ratio $\langle J_f\rangle/\langle J_0\rangle$. The distributions $P_{J_H'}(M_H')$ were used to calculate the out-of-plane γ-ray angular distributions with various dipole-quadrupole admixtures.

A ratio $\langle J_f\rangle/\langle J_0\rangle = 0.9$ is necessary in order to reproduce the measured γ-ray anisotropy if there are two dipole transitions. This value is almost independent of the Z of the projectile-like fragments as shown by the full-drawn line of Fig. 18(c). The calculation not only reproduces the γ-ray anisotropy but it also gives good agreement for the relative width [Fig. 18(a)]. The skewness, although still too large, has the right trend [Fig. 18(b)]. A calculation assuming the same amount of dipole-quadrupole admixture and a ratio $\langle J_f\rangle/\langle J_0\rangle = 1.2$ is illustrated by the dashed-dotted curve of Fig. 18(c). This increase in the fluctuating component gives a better agreement with the experimental anisotropy for the largest values of the Z of the projectile-like fragment, while the relative width and the skewness are left unchanged. This result could indicate a slight dependence of the fluctuating component of the angular momentum upon the mass asymmetry. Such a large value of

J_f near symmetric mass split increases the value of $\langle J\rangle = \langle|\vec{J}_L| + |\vec{J}_H|\rangle$ for the primary fragments by ~6 $\hbar$ over the sticking value for deformed nuclei (dashed curve in Fig. 15), and may be responsible in part for the discrepancy with the experimental data observed there for $Z^* \geq 15$.

There exist, of course, different combinations of the ratio $\langle J_f\rangle/\langle J_0\rangle$ and of the amount of stretched dipole admixture compatible with the measured γ-ray anisotropy. A decrease in $\langle J_f\rangle/\langle J_0\rangle$ can be compensated by an increase in the dipole admixture. This is illustrated in Fig. 19 where the γ-ray anisotropy A and the relative width (which depends only on $\langle J_f\rangle/\langle J_0\rangle$) are plotted as a function of $\langle J_f\rangle/\langle J_0\rangle$ for different numbers of dipole transitions. The particular case shown is for the $Z=9$ projectile-like fragment detected at 45°. Thus, even for four dipole γ rays (corresponding to ~50% dipole admixture), $\langle J_f\rangle/\langle J_0\rangle = 0.5$ is required to explain the observed anisotropy.

The effect of a random angular momentum on the three-point γ-ray angular correlation for various dipole admixtures is shown in Fig. 20 for $Z=5$, 6, and 9. The curves obtained for a 30% dipole admixture and $\langle J_f\rangle/\langle J_0\rangle = 0.8$–$0.9$ give excellent fits to the data. A 50% dipole admixture and $\langle J_f\rangle/\langle J_0\rangle = 0.5$, while reproducing the anisotropy, are in disagreement with the full angular correlation. On the other hand, a dipole admixture of 20% which may be considered as a lower limit, based on our results for evaporation residues (Fig. 9) and on other work,[52,53,56] places an upper limit of 1.1 on the ratio $\langle J_f\rangle/\langle J_0\rangle$.

The assumption that J_f is proportional to J_0 is extreme, of course, and has been made only for simplicity. Relaxing this hypothesis would increase the predicted value of $\sigma_J/\langle J\rangle$, in better agreement with experiment.

The assumption of uncorrelated orientations for the random component J_f of the angular momentum in the light and heavy fragments, while important for calculating $\sigma_J/\langle J\rangle$ for symmetric mass splits, has little consequence for very asymmetric mass fragmentation in which nearly all of the angular

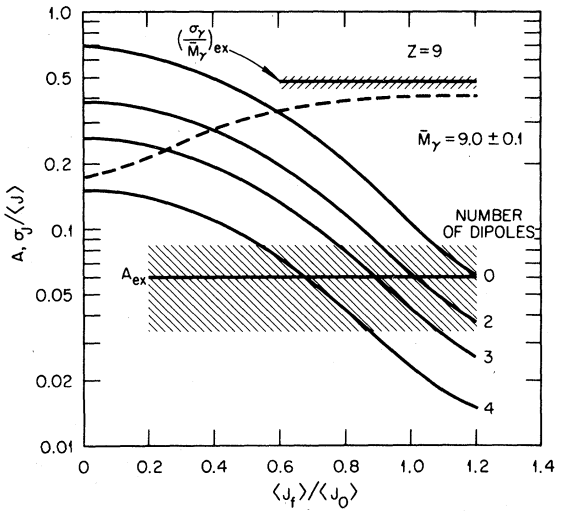

FIG. 19. Dependence of the calculated out-of-plane γ-ray anisotropy A (solid curves) and relative width $\sigma_J/\langle J\rangle$ (dashed curve) on the relative magnitude $\langle J_f\rangle/\langle J_0\rangle$ of the fluctuating component for different dipole-quadrupole admixtures for a projectile-like fragment with $Z=9$ detected at 45°. The experimental values are indicated by the hatched area ($\sigma_J/\langle J\rangle$ is independent of this admixture).

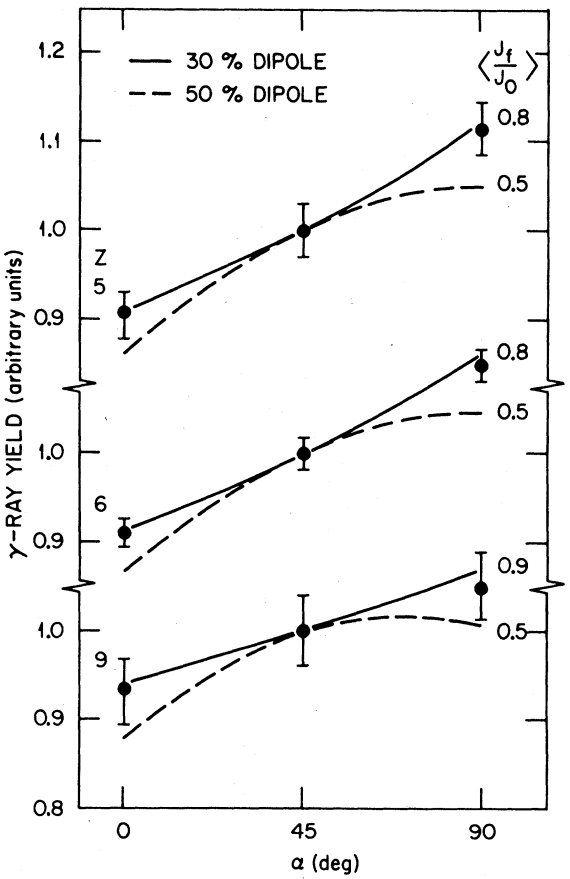

FIG. 20. Out-of-plane γ-ray angular correlations measured for projectile-like fragments with $Z=5$, 6, and 9 detected at 45°. Zero degree corresponds to the direction perpendicular to the reaction plane. The full curves were calculated assuming a 30% dipole admixture and $\langle J_f\rangle/\langle J_0\rangle = 0.8$ for $Z=5$ and 6 and $\langle J_f\rangle/\langle J_0\rangle = 0.9$ for $Z=9$. They give an excellent fit to the experimental data. The dashed curves, calculated with a 50% dipole-quadrupole admixture and $\langle J_f\rangle/\langle J_0\rangle = 0.5$, reproduce the measured γ-ray anisotropy but fail to fit the experimental angular correlations.

momentum is in the heavy partner. Thus, our conclusions are not dependent on this assumption.

The polarization $P_z \equiv \langle M/J \rangle$, the alignment $P_{zz} \equiv \frac{3}{2}\langle (M/J)^2 \rangle - \frac{1}{2}$, and the average depolarization angle $\beta \equiv \cos^{-1}\langle M/J \rangle$ are plotted in Fig. 21 as a function of the ratio $\langle J_f \rangle / \langle J_0 \rangle$. This figure is useful in relating the results of this experiment to other experiments in which the alignment may be expressed in terms other than the ratio of a random component to an aligned component. After considering the various uncertainties in the experiment and the analysis, we assign the value $\langle J_f \rangle / \langle J_0 \rangle = 0.8^{+0.3}_{-0.2}$ which corresponds to $P_z = 0.79^{+0.09}_{-0.20}$, $P_{zz} = 0.46^{+0.20}_{-0.30}$, and $\beta = 38^{\circ}{}^{+15^{\circ}}_{-10^{\circ}}$. (It should be noted that there is a large difference between P_{zz} as defined above and the quantity $\hat{P}_{zz} = \frac{3}{2}\langle M^2 \rangle / \langle J^2 \rangle - \frac{1}{2}$ when P_{zz} deviates significantly from unity. In fact, $P_{zz} = 0.5$ when $\hat{P}_{zz} = 0.25$.)

It is of interest to consider the various mechanisms[30-32] mentioned in the Introduction which might be responsible for a large component of random angular momentum. There is one mechanism for which quantitative expressions are available and which may be applied to the present case in a straightforward manner.

In a recent paper, Moretto and Schmitt[67] have considered the thermal excitation of collective modes such as bending, twisting, wriggling, and tilting. They assume a configuration at scission of two touching spheres of equal mass. The excitation of bending and wriggling modes generates an angular momentum randomly oriented in a plane perpendicular to the separation axis. The excitation of the twisting and tilting modes, however, generates an angular momentum directed along the separation axis. When combined, these different modes produce in each fragment an angular momentum which is to a good approximation randomly oriented. It is this component of angular momentum which may contribute to the loss of the full alignment otherwise expected in the classical picture (sticking) of angular momentum transfer.

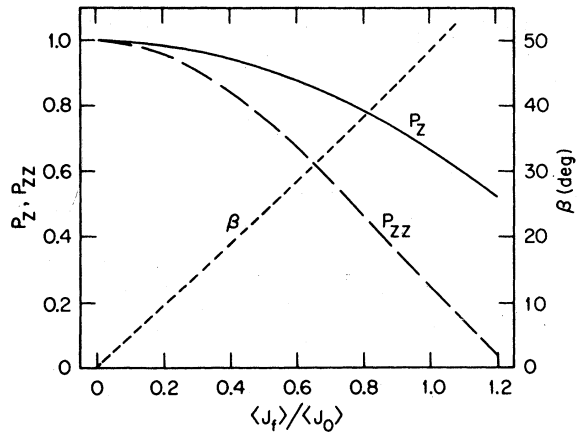

FIG. 21. The relationship of $\langle J_f \rangle / \langle J_0 \rangle$ to the average polarization, defined here by $P_z \equiv \langle M/J \rangle$, with the alignment $P_{zz} = \frac{3}{2}\langle (M/J)^2 \rangle - \frac{1}{2}$ and with the angle β, the rms deviation of the orientation of the transferred angular momentum from the normal to the reaction plane.

The rms value of the randomly oriented angular momentum, summed over both fragments, is given by

$$\langle J_f^2 \rangle^{1/2} = (2 + \sqrt{2})(\mathcal{I}T)^{1/2}, \tag{30}$$

where $\mathcal{I}$ is the moment of inertia of one of the identical fragments and T its temperature. The total average angular momentum imparted to the fragments, defined as the sum of the moduli of the average angular momentum imparted to each fragment, is given by

$$\langle J \rangle = \tfrac{2}{7}\langle l_i \rangle + \frac{14\mathcal{I}T}{\langle l_i \rangle}, \tag{31}$$

where $\langle l_i \rangle$ is the average incident partial wave contributing to strongly damped collisions. The first term on the right in Eq. (31) is the average angular momentum transfer $\langle J_0 \rangle$ expected from sticking, whereas the second term represents the contribution from thermal excitation of the collective modes. The variance of J is given by

$$\sigma_J^{\,2} = (\tfrac{24}{7})\mathcal{I}T, \tag{32}$$

and the depolarization angle is defined as

$$\beta = \sin^{-1}\left(\frac{\langle J_f^2 \rangle^{1/2}}{\langle J_0 \rangle}\right). \tag{33}$$

The different quantities appearing in Eqs. (30) through (33) are calculated as follows: For a symmetric mass split, the total excitation energy before particle emission is ~67 MeV [Fig. 3(b)], which yields an excitation energy $E^* = 34$ MeV per fragment. If we take for the level density parameter $a = A/7.5$ and $A = 42$ for the mass of one fragment, the temperature $T = (E^*/a)^{1/2} = 2.5$ MeV. With $r_0 = 1.4$ fm as the radius parameter the moment of inertia of one fragment $\mathcal{I} = 9.5\ \hbar^2\ \text{MeV}^{-1}$. We have $\langle l_i \rangle = 68\ \hbar$ for the average incident partial wave contributing to completely damped collisions. Thus, using Eqs. (30) to (33), we deduce $\langle J_0 \rangle = 19.4\ \hbar$, $\langle J_f^2 \rangle^{1/2} = 16.4\ \hbar$, $\langle J \rangle = 24.2\ \hbar$, $\beta = 43^{\circ}$, $\sigma_J = 9.0\ \hbar$, and $\sigma_J / \langle J \rangle = 0.37$. The value $\langle J \rangle = 24.2\ \hbar$ is somewhat larger than the value of ~20 $\hbar$ deduced from the γ-ray multiplicity for near-symmetric mass splits (Fig. 15). However, this calculated value could be brought into better agreement with the data by taking into account the effects of deformation in the exit channel. The ratio of the fluctuating to the nonfluctuating

components of the angular momentum, $\langle J_f^2\rangle^{1/2}/\langle J\rangle = 0.85$, is in good agreement with our measurement. Combining quadratically the relative width $\sigma_J/\langle J\rangle = 0.3$ resulting from particle emission alone [Fig. 18(a)] with the predicted relative width $\sigma_J/\langle J\rangle = 0.37$ arising from the fluctuating component of the angular momentum, a value $\sigma_J/\langle J\rangle = 0.47$ is obtained for the J distribution in the fragments prior to γ decay. This is in excellent agreement with the measured width $\sigma_\gamma/\langle M_\gamma\rangle = 0.48$ for the γ-ray distribution. Thus, the thermal excitation of collective modes of angular momentum is a mechanism which can quantitatively account for the random angular momentum deduced in the present experiment.

A microscopic, statistical model of angular momentum transfer has recently been proposed by Vandenbosch.[32] In this picture (as in other models of this general type) the transfer and exchange of individual nucleons through a narrow window connecting the two heavy ions converts part of the orbital motion into intrinsic angular momentum. The Fermi motion of the transferred nucleons is responsible for generating a randomly oriented component of angular momenta. Under the assumptions made, this model is currently most appropriate for quasielastic reactions, i.e., for small energy losses and short interaction times, well before full relaxation is reached.

The effects of zero-point motion of the ground state on the scattering of heavy ions have been considered by Esbensen *et al.*[31] Considering also the fact that ^{20}Ne is a deformed nucleus, there exists the possibility that the initial conditions of the scattering process may be at least partly responsible for a misalignment of the transferred angular momentum. It would be interesting to have quantitative comparisons of these models with the present experimental data.

V. SUMMARY

Energy and angular and charge distribution have been measured for the projectile-like fragments produced in the reaction of 166-MeV ^{20}Ne with ^{63}Cu. These have been analyzed with the phenomenological model of Riedel *et al.*[47] to yield relaxation times for energy and angular momentum dissipation and the charge diffusion coefficient. Measurements of the γ-ray multiplicity, made in coincidence with the reaction products for deep inelastic scattering, enabled a deduction of the transferred angular momentum, the magnitude of which is consistent with the sticking condition for fully relaxed, deformed fragments in the exit channel. The small anisotropy in the probability for γ-ray emission in the reaction plane and perpendicular to the reaction plane may be explained by the introduction of a random component of transferred angular momentum. The deduced magnitude of the fluctuating component is similar to that of the aligned component and also accounts for the large width of the γ-ray multiplicity distribution. The predictions of a model in which a random component of angular momentum is generated via thermal excitations of collective modes of motion are consistent with the experimental results.

ACKNOWLEDGMENTS

We are pleased to acknowledge the help of C. B. Fulmer, R. L. Robinson, and A. H. Snell in the early stages of the experiment. A. Gavron provided valuable assistance with the statistical model calculations. We are pleased to acknowledge helpful comments from W. Nörenberg. This research was sponsored by the U. S. Department of Energy, Division of Basic Energy Sciences, under Contract No. W-7405-eng-26 with Union Carbide Corporation.

---

*Present address: DPh-N/BE, CEN Saclay, BP 2, 91190 Gif-sur-Yvette, France.
†Present address: Building 88, Lawrence Berkeley Laboratory, Berkeley, California 94720.
‡Present address: Institute of Physics, University of Uppsala, Uppsala, Sweden.

[1]W. U. Schröder and J. R. Huizenga, Annu. Rev. Nucl. Sci. 27, 465 (1977) and references therein.
[2]M. Lefort and Ch. Ngô, Ann. Phys. (Paris) 3, 5 (1978) and references therein.
[3]J. Peter, M. Berlanger, C. Ngô, B. Tamain, C. Mazur, M. Ribrag, and C. Signarbieux, Z. Phys. A 283, 413 (1977).
[4]F. Plasil, R. L. Ferguson, H. C. Britt, R. H. Stokes, B. H. Erkkila, P. D. Goldstone, M. Blann, and H. H. Gutbrod, Phys. Rev. Lett. 40, 1164 (1978).
[5]R. Babinet, B. Cauvin, J. Girard, H. Nifenecker, B. Gatty, D. Guerreau, M. Lefort, and X. Tarrago, Nucl. Phys. A296, 160 (1978).
[6]Y. Eyal, A. Gavron, I. Tserruya, Z. Fraenkel, Y. Eisen, S. Wald, R. Bass, G. R. Gould, G. Keyling, R. Renfordt, K. Stelzer, R. Zitzmann, A. Gobbi, U. Lynen, H. Stelzer, I. Rode, and R. Bock, Phys. Rev. Lett. 41, 625 (1978).
[7]D. Hilscher, J. R. Birkelund, A. D. Hoover, W. U. Schröder, W. W. Wilcke, J. R. Huizenga, A. C. Mignerey, K. L. Wolf, H. F. Breuer, and V. E. Viola, Phys. Rev. C 20, 576 (1979).
[8]W. Nörenberg, Phys. Lett. 52B, 289 (1974).
[9]D. H. E. Gross and H. Kalinowski, Phys. Lett. 48B, 302 (1974).
[10]L. G. Moretto and J. S. Sventek, Phys. Lett. 58B, 26

(1975).
[11]K. Siwek-Wilczynska and J. Wilczynski, Nucl. Phys. A264, 115 (1976).
[12]R. Albrecht, W. Dünnweber, G. Graw, H. Ho, S. G. Steadman, and J. P. Wurm, Phys. Rev. Lett. 34, 1400 (1975).
[13]P. Glässel, R. S. Simon, R. M. Diamond, R. C. Jared, I. Y. Lee, L. G. Moretto, J. O. Newton, R. Schmitt, and F. S. Stephens, Phys. Rev. Lett. 38, 331 (1977).
[14]K. Van Bibber, R. Ledoux, S. G. Steadman, F. Videbaek, G. Young, and C. Flaum, Phys. Rev. Lett. 38, 334 (1977).
[15]P. Dyer, R. J. Puigh, R. Vandenbosch, T. D. Thomas, M. S. Zisman, C. Stolk, and J. A. Tjon, Phys. Rev. Lett. 39, 395 (1977).
[16]M. N. Namboodiri, J. B. Natowitz, P. Kasiraj, R. Eggers, L. Adler, P. Gonthier, C. Cerruti, and S. Simon, Phys. Rev. C 20, 982 (1979).
[17]M. M. Aleonard, G. J. Wozniak, P. Glässel, M. A. Deleplanque, R. M. Diamond, L. G. Moretto, R. P. Schmitt, and F. S. Stephens, Phys. Rev. Lett. 40, 622 (1978).
[18]C. Gerschel, M. A. Deleplanque, M. Ishihara, C. Ngô, N. Perrin, J. Peter, B. Tamain, L. Valentin, D. Paya, Y. Sugiyama, M. Berlanger, and F. Hanappe, Nucl. Phys. A317, 473 (1979).
[19]D. V. Harrach, P. Glässel, Y. Civelekoglu, R. Männer, and H. J. Specht, Phys. Rev. Lett. 42, 1728 (1979).
[20]P. R. Christensen, F. Folkmann, O. Hansen, O. Nathan, N. Trautner, F. Videbaek, S. Y. van der Werf, H. C. Britt, R. P. Chestnut, H. Freiesleben, and F. Pühlhofer, Phys. Rev. Lett. 40, 1245 (1978).
[21]A. Olmi, H. Sann, D. Pelte, Y. Eyal, A. Gobbi, W. Kohl, U. Lynen, G. Rudolf, H. Stelzer, and R. Bock, Phys. Rev. Lett. 41, 688 (1978).
[22]R. A. Dayras, R. G. Stokstad, C. B. Fulmer, D. C. Hensley, M. L. Halbert, R. L. Robinson, A. H. Snell, D. G. Sarantites, L. Westerberg, and J. H. Barker, Phys. Rev. Lett. 42, 697 (1979).
[23]M. Berlanger, M. A. Deleplanque, C. Gerschel, F. Hanappe, M. Leblanc, J. F. Mayault, C. Ngô, D. Paya, N. Perrin, J. Peter, B. Tamain, and L. Valentin, J. Phys. Lett. (Paris) 37, L323 (1976).
[24]R. Bock, B. Fischer, A. Gobbi, K. Hildenbrand, W. Kohl, U. Lynen, I. Rode, H. Stelzer, G. Auger, J. Galin, J. M. Lagrange, B. B. Back, and R. Albrecht, Nukleonik 22, 529 (1977).
[25]C. Lauterbach, W. Dünnweber, G. Graw, W. Hering, H. Puchta, and W. Trautmann, Phys. Rev. Lett. 41, 1774 (1978).
[26]H. Puchta, W. Dünnweber, W. Hering, C. Lauterbach, and W. Trautmann, Phys. Rev. Lett. 43, 623 (1979).
[27]W. Trautmann, J. de Boer, W. Dünnweber, G. Graw, R. Kopp, C. Lauterbach, H. Puchta, and U. Lynen, Phys. Rev. Lett. 39, 1062 (1977).
[28]G. Wolschin and W. Nörenberg, Phys. Rev. Lett. 41, 691 (1978).
[29]G. Wolschin, Nucl. Phys. A316, 146 (1979).
[30]G. J. Wozniak, R. P. Schmitt, P. Glässel, R. C. Jared, G. Bizzard, and L. G. Moretto, Phys. Rev. Lett. 40, 1436 (1978).
[31]H. Esbensen, A. Winther, and R. A. Broglia, Phys. Rev. Lett. 41, 296 (1978).
[32]R. Vandenbosch, Phys. Rev. C 20, 171 (1979).
[33]L. Westerberg, D. G. Sarantites, R. Lovett, J. T. Hood, J. H. Barker, C. M. Currie, and N. Mullani, Nucl. Instrum. Methods 145, 295 (1977).
[34]F. E. Obenshain, R. L. Ferguson, M. L. Halbert, D. C. Hensley, H. Nakahara, F. Plasil, F. Pleasonton, A. H. Snell, and R. G. Stokstad, Phys. Rev. C 18, 764 (1978).
[35]F. Plasil and M. Blann, Phys. Rev. C 11, 508 (1975).
[36]R. Bass, Phys. Lett. 47B, 139 (1973).
[37]S. B. Kaufman, E. P. Steinberg, B. D. Wilkins, J. Unik, and A. J. Gorski, Nucl. Instrum. Methods 115, 47 (1974).
[38]L. C. Northcliffe and R. F. Schilling, Nucl. Data Tables A7, 233 (1970).
[39]H. Ho, R. Albrecht, W. Dünnweber, G. Graw, S. G. Steadman, J. P. Wurm, D. Disdier, V. Rauch, and F. Scheibling, Z. Phys. A 283, 235 (1977).
[40]J. W. Harris, T. M. Cormier, D. F. Geesaman, L. L. Lee, R. L. McGrath, and J. P. Wurm, Phys. Rev. Lett. 38, 1460 (1977).
[41]J. M. Miller, G. L. Catchen, D. Logan, M. Rajagopalan, J. M. Alexander, M. Kaplan, and M. S. Zisman, Phys. Rev. Lett. 40, 100 (1978).
[42]R. K. Bhowmik, E. C. Pollacco, N. E. Sanderson, J. B. A. England, and G. C. Morrison, Phys. Rev. Lett. 43, 619 (1979).
[43]Monte Carlo statistical-model code JULIAN, M. Hillman and Y. Eyal, modified by A. Gavron to couple angular momentum projections.
[44]J. Galin, J. Phys. 37, C5-83 (1976).
[45]J. Galin, L. G. Moretto, R. Babinet, R. Schmitt, R. Jared, and S. G. Thompson, Nucl. Phys. A255, 472 (1975).
[46]L. G. Moretto, S. K. Kataria, R. C. Jared, R. Schmitt, and S. G. Thompson, Nucl. Phys. A255, 491 (1975).
[47]G. Wolschin and W. Nörenberg, Z. Phys. A 284, 209 (1978); C. Riedel, G. Wolschin, and W. Nörenberg, *ibid.* 290, 47 (1979).
[48]S. Ayik, G. Wolschin, and W. Nörenberg, Z. Phys. A 286, 271 (1978).
[49]A. Gobbi and W. Nörenberg, *Heavy-Ion Collisions*, edited by R. Bock (North-Holland, Amsterdam, in press); W. Nörenberg, private communication.
[50]M. V. Banaschik, R. S. Simon, P. Colombani, D. P. Soroka, F. S. Stephens, and R. M. Diamond, Phys. Rev. Lett. 34, 892 (1975).
[51]J. F. Mollenauer, Phys. Rev. 127, 867 (1962).
[52]J. J. Simpson, P. O. Tjøm, I. Espe, G. B. Hagemann, B. Herskind, and M. Neiman, Nucl. Phys. A287, 362 (1977).
[53]D. G. Sarantites, L. Westerberg, M. L. Halbert, R. A. Dayras, D. C. Hensley, and J. H. Barker, Phys. Rev. C 18, 774 (1978).
[54]C. F. Tsang, Phys. Scr. 10A, 90 (1974).
[55]R. A. Broglia, C. H. Dasso, and A. Winther, Phys. Lett. 61B, 113 (1976).
[56]M. A. Deleplanque, Th. Byrski, R. M. Diamond, H. Hübel, F. S. Stephens, B. Herskind, and R. Bauer, Phys. Rev. Lett. 41, 1105 (1978).
[57]J. H. Degnan, B. L. Cohen, G. R. Rao, K. C. Chan, and L. Shabason, Phys. Rev. C 8, 2255 (1973).
[58]J. H. Barker, D. G. Sarantites, Ö. Skeppstedt, E. Wallander, G. Alenius, and S.-E. Arnell, Phys. Rev. C 18, 119 (1978).
[59]K. A. Geoffroy, J. B. Natowitz, R. C. Eggers, and M. N. Namboodiri, Nucl. Phys. A302, 310 (1978).
[60]K. A. Geoffroy, J. B. Natowitz, R. Eggers, P. Kasiraj,

and M. N. Namboodiri, Nucl. Phys. A302, 333 (1978).
[61]B. B. Back and S. Bjørnholm, Nucl. Phys. A302, 343 (1978).
[62]O. Andersen, R. Bauer, G. B. Hagemann, M. L. Halbert, B. Herskind, N. Neiman, H. Oeschler, and H. Ryde, Nucl. Phys. A295, 163 (1978).
[63]C. M. Perey and F. G. Perey, Nucl. Data Tables 17, 1 (1976).
[64]J. R. Huizenga and G. Igo, Nucl. Phys. 29, 462 (1962).
[65]A. Gilbert and A. G. W. Cameron, Can. J. Phys. 43, 1446 (1965).
[66]F. Bertrand, M. Martinot, and N. Verges, in *Nuclear Data in Science and Technology* (IAEA, Vienna, 1973), Vol. II, p. 353.
[67]L. G. Moretto and R. P. Schmitt, Phys. Rev. C 21, 204 (1980).